

Small- x Physics: From HERA to LHC and beyond

Leonid Frankfurt

School of Physics and Astronomy, Tel Aviv University, 69978 Tel Aviv, Israel

Mark Strikman

Department of Physics, Pennsylvania State University, University Park, PA 16802, USA

Christian Weiss

Theory Group, Jefferson Lab, Newport News, VA 23606, USA

Abstract

We summarize the lessons learned from studies of hard scattering processes in high-energy electron-proton collisions at HERA and antiproton-proton collisions at the Tevatron, with the aim of predicting new strong interaction phenomena observable in next-generation experiments at the Large Hadron Collider (LHC). Processes reviewed include inclusive deep-inelastic scattering (DIS) at small x , exclusive and diffractive processes in DIS and hadron-hadron scattering, as well as color transparency and nuclear shadowing effects. A unified treatment of these processes is outlined, based on factorization theorems of quantum chromodynamics, and using the correspondence between the “parton” picture in the infinite-momentum frame and the “dipole” picture of high-energy processes in the target rest frame. The crucial role of the three-dimensional quark and gluon structure of the nucleon is emphasized. A new dynamical effect predicted at high energies is the unitarity, or black disk, limit (BDL) in the interaction of small dipoles with hadronic matter, due to the increase of the gluon density at small x . This effect is marginally visible in diffractive DIS at HERA and will lead to the complete disappearance of Bjorken scaling at higher energies. In hadron-hadron scattering at LHC energies and beyond (cosmic ray physics), the BDL will be a standard feature of the dynamics, with implications for (a) hadron production at forward and central rapidities in central proton-proton and proton-nucleus collisions, in particular events with heavy particle production (Higgs), (b) proton-proton elastic scattering, (c) heavy-ion collisions. We also outline the possibilities for studies of diffractive processes and photon-induced reactions (ultraperipheral collisions) at LHC, as well as possible measurements with a future electron-ion collider.

PACS numbers: 11.80.La, 12.40.Gg, 12.40.Pp, 25.40.Ve, 27.75.+r

Key Words: High-energy scattering, quantum chromodynamics, diffraction, hadronic final states

Contents

1	Introduction	3
2	QCD factorization and the space-time evolution of small-x scattering	7
2.1	QCD factorization of hard processes	7
2.2	Space-time evolution of small- x scattering in the target rest frame	9
3	Inclusive γ^*p scattering at small x	13
3.1	DGLAP evolution and the HERA data	13
3.2	Space-time picture of inclusive DIS	15
3.3	Breakdown of the DGLAP approximation at very small x	17
4	Exclusive processes in γ^*p scattering at small x	19
4.1	QCD factorization for hard exclusive processes	19
4.2	Space-time picture of hard exclusive processes	20
4.3	Vector meson production at HERA	22
4.4	Transverse spatial distribution of gluons in the nucleon	24
4.5	Color transparency in hard processes with nuclei	26
5	Diffraction in γ^*p scattering	27
5.1	QCD factorization for hard diffractive processes	27
5.2	Space-time picture of hard diffractive processes	29
5.3	Diffraction and leading-twist nuclear shadowing	31
5.4	Implications of nuclear shadowing for heavy-ion collisions	32
6	Black-disk limit in dipole-hadron interactions	33
6.1	Violation of the leading-twist approximation at small x	33
6.2	Theoretical issues in describing the black-disk limit	35
6.3	High-energy limit of nuclear and hadronic structure functions	36
6.4	Black-disk limit in hard diffractive scattering from heavy nuclei	38

7	Small-x dynamics in hadron-hadron collisions	39
7.1	Transverse radius of hard and soft interactions	39
7.2	Black-disk limit in high-energy pA and pp collisions	42
7.3	Final state properties in central pp collisions at LHC	45
7.4	Black-disk limit in elastic pp scattering	47
7.5	Ion-induced quark-gluon implosion	49
7.6	Cosmic ray physics near the GZK cutoff	49
8	Hard diffraction at hadron colliders	50
8.1	Diffractive proton dissociation into three jets	50
8.2	Exclusive diffractive Higgs production	51
8.3	Inclusive hard diffractive processes	52
9	Summary and Outlook	53
9.1	From HERA to LHC	53
9.2	Measurement of parton densities in pp and pA collisions at LHC	54
9.3	Small- x phenomena in ultraperipheral collisions at LHC	55
9.4	Small- x physics at RHIC and an electron-ion collider	56

1 Introduction

In understanding the nature of strong interactions, progress has mostly come from the investigation of certain “extreme” kinematic regions, in which the dynamics simplifies. One such region is high-energy hadron-hadron scattering, in which the center-of-mass energy is significantly larger than the masses of the hadronic systems in the initial and final state. Historically, this was the first area in which powerful mathematical methods, such as dispersion relations and Reggeon calculus, could be applied to strong interaction phenomena. They are based on the general principles of unitarity of the scattering matrix (conservation of probability) and analyticity of scattering amplitudes (causality). These methods have given us important insights into general properties of high-energy processes, such as the increase of the radius of interaction with energy predicted by V. Gribov [1, 2], the Froissart bound for the growth of total hadronic cross sections with energy [3], and the Pommeranchuk theorem of asymptotic equality of particle-particle and particle-antiparticle cross sections.

Further progress came with the study of “hard” scattering processes, characterized by a momentum transfer significantly larger than the typical mass scale associated with hadron structure, μ (a reasonable numerical value for this scale is the ρ meson mass). Such processes can be described in quantum chromodynamics (QCD), the field theory of interacting quarks and gluons, the fundamental property of which is the smallness of the effective coupling constant in small space-time intervals (asymptotic freedom) [4, 5]. Hard processes happen so “rapidly” that they do not significantly change the environment of the interacting quarks and gluons inside the hadrons. This allows one to calculate their amplitudes using a technique called factorization — a systematic separation into a hard quark-gluon scattering process and certain functions describing the distribution of quarks and gluons in the participating hadrons. The simplest such process is deep-inelastic lepton-hadron scattering (DIS) in the so-called Bjorken limit, $Q^2 \sim W^2 \gg \mu^2$, see Fig. 1. Historically, the observation of scaling behavior in the structure functions of inclusive DIS [6] gave the first indication of the presence of quasi-free, pointlike constituents in the proton [7]. Another class of processes for which factorization is possible are certain hard processes in hadron-hadron scattering, such as the production of jets with large transverse momenta or large-mass dilepton pairs.

A particularly interesting region of strong interactions are hard scattering processes in the region where the center-of-mass energy becomes large compared to the momentum transfer, $W^2 \gg Q^2 \gg \mu^2$. In DIS this limit corresponds to values of the Bjorken variable $x \ll 1$ (see Fig. 1), whence this field is known as “small- x physics.” On one hand, because of the large momentum transfer, such processes probe the quark and gluon degrees of freedom of QCD. On the other hand, they share many characteristics with high-energy hadron-hadron scattering, such as a large spatial extension of the interaction region along the collision axis (this will be explained in detail in Sec. 2.2). The treatment of such processes generally requires a combination of the methods of QCD factorization and “pre-QCD” methods of high-energy hadron-hadron scattering for modeling the dynamics of the hadronic environment of the quarks and gluons participating in the hard process. From the point of view of QCD, the high-energy (small- x) region corresponds to a greatly increased phase space for gluon radiation as compared to $x \sim 1$. QCD predicts a fast rise of the gluon density in the nucleon with decreasing x , and thus a strong increase of the DIS cross section with energy [8, 9]. A challenging question, which is presently being addressed in different approaches, is the role of unitarity of the scattering matrix

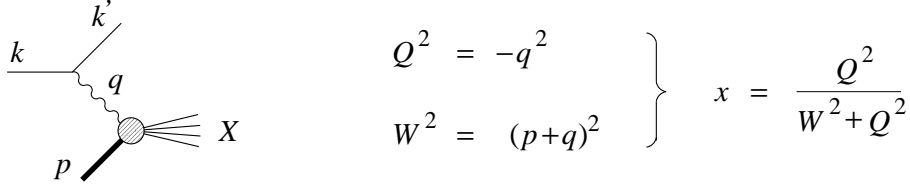


Figure 1: The kinematics of deep–inelastic lepton–hadron scattering (DIS). The interaction proceeds by exchange of a virtual photon, whose four–momentum is given by the difference of the lepton momenta, $q = k' - k$. The hadronic scattering process is characterized by two kinematic invariants, the photon virtuality, $q^2 \equiv -Q^2 < 0$, and the photon–proton center–of–mass energy, W , or, alternatively, the Bjorken scaling variable, x . (We neglect the target mass.)

in such processes at high energies. More generally, one hopes to eventually understand the quark–gluon dynamics underlying such general high–energy phenomena as the growth of the radius of interaction with energy, and the Froissart bound. This dynamics would correspond to a strongly interacting quark–gluon system at small coupling constant, and represent a fascinating new form of “QCD matter” which could be produced in the laboratory.

An intuitive understanding of the dynamics of hard scattering processes and the basis for QCD factorization can be developed by following the space–time evolution of the reactions in certain reference frames. At high energies (small x), the space–time evolution of DIS can be discussed in two complementary ways. In a frame where the proton is fast–moving one obtains the well–known parton picture of hard processes, in which the hard scattering process involves quarks and gluons carrying a certain fraction (here, x) of the proton’s momentum. In the proton rest frame, on the other hand, the DIS process takes the form of the scattering of a quark–antiquark dipole from the target, with the dipole formed a long time before reaching the target, and having a distribution of transverse sizes extending down to values $\sim 1/Q$. This representation reveals a close relation between DIS at small x and the so–called “color transparency” phenomenon — the transparency of hadronic matter to the propagation of spatially small color–singlet configurations, as observed *e.g.* in the suppression of the interaction of heavy quarkonia with hadronic matter. The correspondence between the “parton” and the “dipole” picture of small– x processes is a powerful tool for analyzing the dynamics of strong interactions in this regime. (A pedagogical introduction to these concepts will be given in Sec. 2.)

The experimental investigation of small– x processes became possible with the advent of high–energy colliders (colliding beam facilities). Extensive studies of DIS at small x have been performed at the HERA electron–proton (ep) collider at DESY. Measurements of inclusive cross sections have spectacularly confirmed the rise of the gluon density in the proton at small x , as predicted by QCD, down to values $x \sim 10^{-4}$. Measurements of exclusive processes in DIS, such as heavy and light vector meson production ($J/\psi, \rho$), provide information about the spatial distribution of partons in the transverse plane (“generalized parton distributions”) and allow us to construct a three–dimensional image of the quark and gluon structure of the nucleon. Finally, measurements of diffractive processes in DIS, in which the produced hadronic system is separated from the target remnants by a large rapidity gap, allow one to probe the interaction of various small–size color–singlet configurations with the proton in much more detail than inclusive DIS.

Another — potentially much more powerful — laboratory for studying small- x physics are high-energy proton-proton (pp) and antiproton-proton ($\bar{p}p$) colliders, such as LHC at CERN (under construction) and the Tevatron at Fermilab. QCD factorization can be applied to $pp/\bar{p}p$ collisions with hard processes, such as the production of dijets with large transverse momenta or heavy particles (W^\pm bosons, Higgs bosons, *etc.*), which originate from binary collisions of partons in the two colliding hadrons. At LHC, such processes can probe parton distributions down to values of $x \sim 10^{-7}$. Even higher energies are reached in collisions of cosmic-ray particles near the Greisen-Zatsepin-Kuzmin cutoff [10] with atmospheric nuclei. In pp scattering, as compared to ep , one is dealing with collisions of two objects with a complex internal structure. This results *e.g.* in a high probability of multiple hard scattering processes at high energies, and a much richer spectrum of soft hadronic interactions. Thus, while QCD factorization can still be applied to certain hard processes in $pp/\bar{p}p$ collisions, the modeling of the hadronic environment of the quarks and gluons participating in the hard process (or processes) is generally much more challenging than in ep scattering.

This review is an attempt to summarize what has been learned about small- x physics from experiments at HERA and the Tevatron and related theoretical studies, and use this information to make predictions for new QCD phenomena observable at LHC. With LHC about to be commissioned, and the HERA program nearing completion, this is a timely exercise. It is not our aim to give a comprehensive overview of the existing collider experiments and their numerous implications for our understanding of QCD. Rather, we identify certain specific “lessons” which are of particular importance in making the transition from HERA to LHC:

- *Black-disk limit in dipole-hadron interactions.* Because of the fast rise of the gluon density at small x , the strength of interaction of small color-singlet configurations (dipoles) with hadronic matter can approach the maximum value allowed by s -channel unitarity. We quantify this effect by formulating an optical model of dipole-hadron scattering, in which the unitarity limit corresponds to the scattering from a “black disk”, whose radius increases with energy (black disk limit, or BDL). We argue that the onset of the BDL regime can be seen in the diffractive DIS data at the upper end of the HERA energy range, as well as in elastic $pp/\bar{p}p$ scattering at Tevatron energies. In DIS at higher energies, the BDL leads to a breakdown of Bjorken scaling. In hadron-hadron collisions at LHC energies and beyond (cosmic ray physics), the dynamics will be deep inside the BDL regime, with numerous consequences for the hadronic final states.
- *Small transverse area of leading partons.* Studies of hard exclusive processes at HERA show that partons in the nucleon with $x > 10^{-2}$ and significant transverse momenta are concentrated in a small transverse area, $\ll 1 \text{ fm}^2$, substantially smaller than the area associated with the nucleon in soft (hadronic) interactions at high energies. The resulting “two-scale picture” of the transverse structure of the nucleon is essential for modeling the hadronic environment of the colliding partons in high-energy pp collisions with hard processes.

Based on these observations, we make several predictions for new strong interaction phenomena observable in pp , pA (proton-nucleus), and AA (nucleus-nucleus) collisions at LHC:

- *Hard processes as a trigger for central pp collisions.* In pp scattering at LHC, hard QCD processes involving binary collisions of partons with momentum fractions $x_{1,2} > 10^{-2}$ occur practically only in pp events with small impact parameters (central collisions). This makes it possible to trigger on central pp events by requiring the presence of a hard dijet (or double dijet) at small rapidities.
- *Black-disk limit in central $pp/pA/AA$ collisions at LHC.* The approach to the BDL at high energies will strongly affect the dynamics of central $pp/pA/AA$ collisions at LHC energies and above. A crucial point is that in hadron-hadron collisions at such energies one is dealing mostly with gluon-gluon dipoles, whose cross section for scattering from hadronic matter is $9/4$ times larger than that of the quark-antiquark dipoles dominating ep scattering. We argue that as a consequence of the approach to the BDL the leading partons in central pp collisions will acquire large transverse momenta ($p_{\perp}^2 \sim$ several 10 GeV^2) and fragment independently, resulting in the disappearance of leading hadrons with small transverse momenta at forward/backward rapidities, increased energy loss, and increased soft particle production at central rapidities. These observable effects allow for experimental studies of this fascinating new regime of “strong gluon fields” at LHC. We also outline the role of the BDL in heavy-ion collisions and cosmic ray physics.
- *Diffraction in high-energy pp collisions.* LHC offers the possibility to study a wide variety of diffractive processes in high-energy pp scattering, which probe the interaction of small-size color singlets with hadronic matter and can be used to map the gluon distribution in the proton. Such processes involve a delicate interplay between hard (partonic) and soft (hadronic) interactions. A crucial ingredient in understanding the dynamics is the information about the transverse spatial distribution of gluons obtained from exclusive vector meson production in DIS at HERA.

We also comment on the potential of LHC for parton distribution measurements at small x , and for studies of small- x dynamics via photon-induced reactions in ultraperipheral $pp/pA/AA$ collisions. Finally, we discuss the opportunities for studies of small- x dynamics provided by the planned electron-ion collider.

The primary purpose of LHC is the search for new heavy particles (Higgs bosons, supersymmetry) in high-energy pp collisions. The small- x phenomena we describe here directly impact on this program. Heavy particles are produced in hard partonic collisions. For the reason described above, the production of heavy particles in inelastic pp collisions happens predominantly in central collisions, which are strongly affected by the approach to the BDL, and the strong interaction background may be completely different from what one would expect based on the naive extrapolation of existing data (Tevatron). Likewise, the search for Higgs bosons in diffractive pp events depends crucially on the understanding of the strong interaction dynamics in these processes.

2 QCD factorization and the space-time evolution of small- x scattering

2.1 QCD factorization of hard processes

We begin by introducing the basic concept of QCD factorization of hard processes, and outlining the space-time evolution of small- x scattering processes at high energies. Our main point is the correspondence between the “parton” picture of hard processes in a frame in which the nucleon is moving fast, and the “dipole” picture of high-energy processes in the target rest frame. In this Section we illustrate this correspondence using as an example the simplest high-energy process, inclusive DIS at small x . Below we shall apply these results to analyze the HERA DIS data (Sec. 3), and generalize them to processes with exclusive (Sec. 4) and diffractive (Sec. 5) final states. The correspondence between the two pictures plays a crucial role in formulating the approach to the unitarity limit at high energies (Sec. 6), and for understanding the dynamics of high-energy hadron-hadron collisions (Secs. 7 and 8).

DIS is essentially the scattering of a virtual photon (γ^*) from a hadronic target, see Fig. 1. By the optical theorem of quantum mechanics, the total γ^*p cross section is given by the imaginary part of the forward scattering amplitude (virtual Compton amplitude), see Fig. 2a. We consider the Bjorken limit, in which both the photon virtuality and the γ^*p center-of-mass energy become large compared to the typical hadronic mass scale, $Q^2 \sim W^2 \gg \mu^2$. As a consequence of the asymptotic freedom of QCD, DIS in this limit can be described as the scattering of the virtual photon from quasi-free quarks (and antiquarks) in the proton. In the simplest approximation, one neglects the interactions of the quarks altogether, and considers the scattering from a free quark, see Fig. 2b. This is equivalent to the space-time picture of DIS expressed in the parton model [7]. Its basic assumption is that, in a reference frame where the proton moves with a large velocity, the interaction of the γ^* with the quarks (“partons”) is instantaneous compared to the characteristic time of their internal motion in the proton. In this picture, the total cross section for γ^*p scattering in the Bjorken limit is given by

$$\sigma^{\gamma^*p \rightarrow X}(Q^2, W) = \frac{4\pi^2\alpha_{\text{em}}}{Q^2(1-x)} F_2(x), \quad F_2(x) = \sum_f e_f^2 x [q_f(x) + \bar{q}_f(x)], \quad (1)$$

where α_{em} is the electromagnetic fine structure constant. Here, e_f are the quark charges ($f = u, d, s \dots$ labels the quark flavor), and $q_f(x)$ and $\bar{q}_f(x)$ are the parton densities, describing the number density of quarks and antiquarks carrying a fraction, x , of the fast-moving proton’s momentum. The transverse momenta of the quarks and antiquarks are of the order $k_{\perp}^2 \sim \mu^2$, and are integrated over. Eq. (1) exhibits the famous property of Bjorken scaling [6], *i.e.*, the structure function, F_2 , depends on the kinematic invariants characterizing the initial state only through the dimensionless Bjorken variable (we neglect the nucleon mass),

$$x \equiv \frac{Q^2}{W^2 + Q^2}. \quad (2)$$

This is a direct consequence of the scattering from pointlike, quasi-free particles.

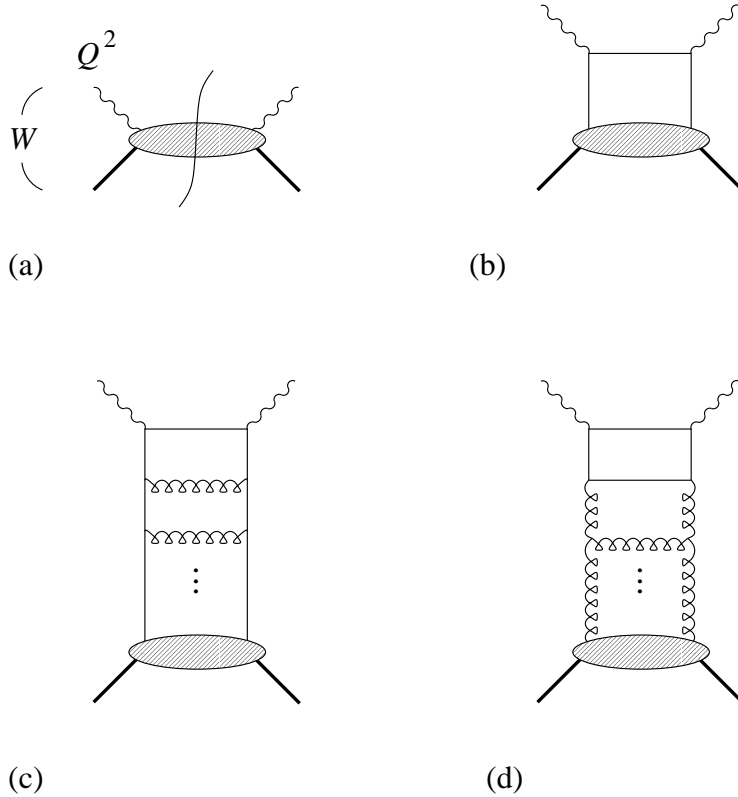


Figure 2: (a) The total cross section for γ^*p scattering is given by the imaginary part of the forward scattering amplitude. (b) The total cross section in the parton model (Bjorken scaling). (c,d) QCD radiative corrections, giving rise to the leading scaling violations in $\alpha_s \ln(Q^2/Q_0^2)$.

The parton model assumption of widely different timescales for the γ^* -quark interaction and the internal motion of the quarks in the proton becomes invalid in quantum field theory, where the ultraviolet divergences introduce a scale larger than Q^2 . At its most elementary, this is the reason why Bjorken scaling is violated in quantum chromodynamics — an argument originally due to V. Gribov. The leading scaling violations in $\alpha_s \ln(Q^2/Q_0^2)$ arise from gluon bremsstrahlung, as described by the ladder-type Feynman diagrams shown in Fig. 2c and d, and can be summed up in closed form. Here, α_s is the strong coupling constant, and Q_0^2 is an arbitrarily chosen initial scale in the region of approximate Bjorken scaling. The result can be expressed in the form of a Q^2 -dependence of the parton densities, governed by a differential equation, the Dokshitzer–Gribov–Lipatov–Altarelli–Parisi (DGLAP) evolution equation [11, 12, 9]. This formulation allows one to retain the basic space–time picture of the parton model while incorporating QCD radiative corrections by way of a Q^2 -dependence of the parton densities. Note that through evolution the gluon density in the proton effectively enters into the structure functions of γ^*p scattering, see Fig. 2d.

The basic structure of the γ^*p total cross section in the Bjorken limit in QCD is that of a product of a “hard” photon–parton cross section (involving virtualities $\sim Q^2$) and a “soft” matrix element (involving virtualities $\sim \mu^2$), describing the distribution of partons in the proton. QCD radiative corrections can be incorporated by a systematic redefinition of the “hard”

and “soft” factors. This property is referred to as factorization. Factorization for the γ^*p total cross section in QCD has been formally demonstrated in several different approaches, including operator methods in which the parton densities appear as nucleon matrix elements of certain non-local light-ray operators, and the evolution equations coincide with the QCD renormalization group equations for these operators. The calculations have also been extended to sum up next-to-leading (NLO) corrections in $\alpha_s \ln(Q^2/Q_0^2)$. We shall see below that the basic technique of factorization can be applied also to exclusive (Sec. 4) and diffractive (Sec. 5) final states in γ^*p scattering, as well as to certain hard processes in hadron–hadron scattering (Sec. 7).

More generally, QCD factorization allows one to perform an asymptotic expansion of the DIS structure functions in the Bjorken limit. The contribution from the diagram of Fig. 2b, Eq. (1), determines the leading power behavior at large Q^2 , with an additional logarithmic dependence appearing due to radiative corrections, Fig 2c and d. In the context of operator methods this is known as the leading–twist approximation. Power corrections of the order μ^2/Q^2 (higher–twist corrections) arise from taking into account the effect of the quark transverse momentum on the hard scattering process and the interaction of the “struck” quark with the non-perturbative gluon field in the proton; the two effects are intimately related because of gauge invariance in QCD [13].

From a mathematical perspective, Bjorken scaling of the moments of the DIS structure functions can be seen as a consequence of the conformal invariance of the QCD Lagrangian. The ultraviolet divergences associated with radiative corrections give rise to anomalous representations of the conformal group, with a logarithmic scale dependence. Later we shall see that at high energies a new dynamical scale appears in QCD, related to the gluon density in the nucleon and its transverse area, which breaks the conformal invariance, and thus leads to the complete disappearance of Bjorken scaling — the black disk limit (BDL), see Sec. 6.

2.2 Space–time evolution of small– x scattering in the target rest frame

We now turn to DIS at high energies, $W^2 \gg Q^2 \gg \mu^2$, which corresponds to values of the Bjorken variable $x \ll 1$. While this processes can be discussed within the standard QCD factorization approach described above, one faces the practical question at which point higher–twist ($1/Q^2$ –) corrections enhanced at small x , or radiative corrections beyond the DGLAP approximation giving rise to factors $\ln(1/x)$, become important. These and other questions can be addressed in a transparent way by considering the time evolution of DIS in the target rest frame, where the process takes the form of the scattering of a small–size $q\bar{q}$ dipole from a hadronic target. More generally, this formulation suggests a new understanding of QCD factorization, closely related to the so–called “color transparency” phenomenon observed in diffractive processes in hadron–hadron scattering.

QCD factorization in DIS and the DGLAP approximation have been formulated using the covariant language of Feynman diagrams. A typical Feynman diagram relevant at small x is shown in Fig. 3a. In order to arrive at a space–time interpretation one needs to perform the integration over the “energy” variable using the residue theorem. It is this step which actually introduces the dependence of the amplitudes on the reference frame. Alternatively, one may directly trace the space–time evolution using the language of time–ordered perturbation theory.

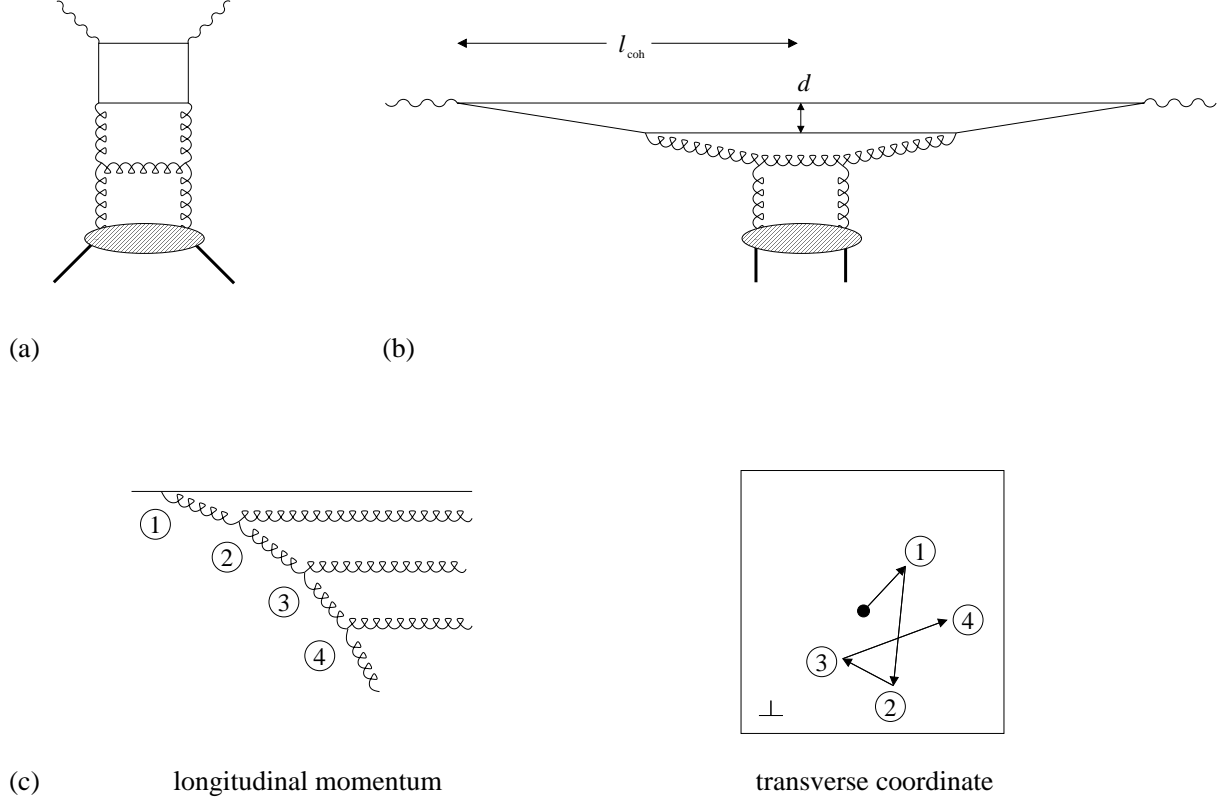


Figure 3: (a) A typical Feynman diagram for inclusive γ^*p scattering at small x . (b) Time evolution of small- x scattering in the target rest frame. (c) The decay of a fast parton in the $q\bar{q}$ dipole. The degradation of longitudinal momenta is accompanied by a random walk in the transverse coordinate.

In this formulation, the time scales of the processes are determined by the energy denominators associated with the various transitions, via the energy–time uncertainty relation, $\Delta t = 1/\Delta E$.

In the target rest frame, the virtual photon in DIS at small x moves with 3-momentum $P \approx Q^2/(2m_N x)$. Consider its conversion into a $q\bar{q}$ pair with longitudinal momenta zP and $(1-z)P$ and transverse momenta $\pm \mathbf{k}_\perp$ (“longitudinal” and “transverse” are defined relative to the direction of motion of the photon). The energy denominator for this transition is

$$\Delta E = \frac{M_{q\bar{q}}^2 + Q^2}{2P}, \quad (3)$$

where $M_{q\bar{q}}^2 \equiv (m_q^2 + k_\perp^2)/[z(1-z)]$ is the invariant mass of the $q\bar{q}$ pair (m_q is the quark mass, $k_\perp \equiv |\mathbf{k}_\perp|$). For a longitudinally polarized photon, the dominant contribution to the cross section comes from values $z \sim 1/2$ and $k_\perp \sim Q$, for which $M_{q\bar{q}}^2 \sim Q^2$ (this will be explained in more detail in Sec. 3.2). For such values the time associated with the $\gamma^* \rightarrow q\bar{q}$ transition is

$$\Delta t = 1/\Delta E \sim Q^2/P \approx 1/(2m_N x). \quad (4)$$

At small x , the photon converts into a $q\bar{q}$ pair long before reaching the target, as illustrated in Fig. 3b. Both the quark and antiquark move essentially with the speed of light. The distance

between the point of their creation and the target, the so-called coherence length, is given by

$$l_{\text{coh}} = c\Delta t. \quad (5)$$

It is important to realize that the $q\bar{q}$ wave packet remains well localized in the longitudinal direction as it travels towards the target, and that the transverse separation between the quark and antiquark (at a given time) is a meaningful concept. It is generally of the order $d \sim 1/M_{q\bar{q}} \sim 1/Q$, and thus small if Q^2 is sufficiently large.

In short, high-energy γ_L^* -hadron scattering in the target rest frame is essentially the scattering of a small-size $q\bar{q}$ dipole from the target hadron. In this formulation, the quantity describing the strong interaction effects is the cross section for dipole-hadron scattering. It can be computed using methods of QCD factorization, with the dipole size, $d \ll \mu$ acting as the factorization scale, see Sec. 3.2. Without going into details, we can immediately state an important property of the cross section, namely that in the limit $d \rightarrow 0$ it vanishes as

$$\sigma^{q\bar{q}\text{-hadron}} \propto d^2, \quad (6)$$

up to logarithmic corrections in d . Eq. (6) reflects a fundamental property of QCD as a gauge theory — the interaction of a small-size color singlet object with hadronic matter is small (“color transparency”). In this understanding of QCD factorization, high-energy γ^* -hadron scattering exhibits a close relation to the interaction of heavy quarkonia with hadronic matter and a number of other color transparency phenomena in hadron-hadron scattering.

To make the dipole picture quantitative, one has to take into account the effects of QCD radiation. In particular, this is necessary in order to determine the coefficient in Eq. (6) with logarithmic accuracy. The importance of different types of radiation can again be studied using the language of time-ordered perturbation theory in the target rest frame. The characteristic time for the quark to radiate a gluon with longitudinal momentum fraction x_g and transverse momentum $\mathbf{k}_{\perp,g}$, relative to the time the $q\bar{q}$ pair spends between its creation and “hitting” the target, (4), is (cf. Fig. 3b)

$$\frac{\Delta t_1}{\Delta t} = \left[Q^2 + \frac{m_q^2 + k_{\perp}^2}{z(1-z)} \right] / \left[Q^2 + \frac{m_q^2 + k_{\perp}^2}{1-z} + \frac{m_q^2 + (\mathbf{k}_{\perp} - \mathbf{k}_{\perp,g})^2}{z-x_g} + \frac{k_{\perp,g}^2}{x_g} \right]. \quad (7)$$

If x is sufficiently small, and for average values of z , the emission process can be repeated several times before the evolved system reaches the target.

There exist several kinematic domains where gluon emission during the propagation of the $q\bar{q}$ wave packet is likely because of a large phase space at small x . One is the emission of partons with transverse momenta smaller than k_{\perp} of the parent parton. Each such emission contributes a factor $\alpha_s \ln(Q^2/Q_0^2)$ in the amplitude, where the logarithm arises from the integration over the phase volume of the radiated gluon. In the standard QCD description of DIS, these are the radiative corrections summed up by the DGLAP evolution equations for the parton distributions described above [11, 12, 9] (see also Ref. [14]). In the context of the dipole picture at small x , the summation of these corrections in leading order (LO) corresponds to a dipole-hadron cross section of the form [15, 16, 17]

$$\sigma^{q\bar{q}\text{-hadron}}(x, d^2) = \frac{\pi^2}{4} F^2 d^2 \alpha_s(Q_{\text{eff}}^2) xG(x, Q_{\text{eff}}^2). \quad (8)$$

Here $F^2 = 4/3$ is the Casimir operator of the fundamental representation of the $SU(3)$ gauge group. Furthermore, $\alpha_s(Q_{\text{eff}}^2)$ is the LO running coupling constant and $G(x, Q_{\text{eff}}^2)$ the LO gluon density in the target. They are evaluated at a scale $Q_{\text{eff}}^2 \propto d^{-2}$. The coefficient of proportionality is not fixed within the LO approximation, and needs to be determined from NLO calculations or from phenomenological considerations, see Sections 3.2 and 4.¹

Eq. (8) actually quotes a simplified expression for the dipole–hadron cross section. The original expression involves an integral over the gluon momentum fractions, which is concentrated in a narrow range above x . Also neglected in Eq. (8) is the contribution proportional to the quark/antiquark distribution in the target, which at small x is suppressed compared to the gluon distribution. This contribution would lead to a flavor dependence of the dipole–nucleon cross section [19].

Another large contribution, specific to small x , comes from the large phase space in rapidity ($\propto z_g$) for emission of gluons without strong degrading of transverse momenta in the leading approximation. Such emissions give rise to factors $\alpha_s(N_c/2\pi)\Delta y$, where $N_c = 3$ is the number of colors in QCD, and $\Delta y = (y_i - y_{i+1})$ is the difference in rapidities between successive partons in the ladder. In terms of x , this corresponds to corrections proportional to $\ln(x_0/x)$, where $x_0 \sim 0.1$ accounts for the fact that nucleon fragmentation enters in the definition of the gluon density in the nucleon and does not produce a logarithm in x . If the rapidity interval for emissions (*i.e.*, the lifetime of the quark–gluon system) becomes very large, one needs to sum these logarithms in addition to the $\alpha_s \ln(Q^2/Q_0^2)$ terms [20], see Sec. 3.3.

QCD radiation generally leads to an increase of the transverse size of the “dressed” dipole with decreasing x , and thus to an increase of the radius of the dipole–hadron interaction with energy. Each individual emission shifts the transverse coordinate of the radiating parton by $\Delta\rho \sim 1/k_\perp$, see Fig. 3c. If there are n successive emissions with comparable, randomly oriented k_\perp (this is the case in the limit of large $\ln x$), the overall shift is [2]

$$\Delta\rho^2 = n/k_\perp^2 = y/(\Delta y k_\perp^2), \quad (9)$$

where y is the rapidity of the initial parton. A similar diffusion mechanism for soft partons was discussed by V. Gribov as a model for the increase of the radius of soft hadronic interactions with energy [1, 2]. In the case of hard processes such as γ^* –hadron scattering, in the region where the DGLAP approximation is valid, the rate of expansion with energy is much smaller than for soft interactions, because of the larger transverse momenta of the emitted partons and the larger rapidity intervals between the emissions. This manifests itself *e.g.* in a much weaker energy dependence of the t –slope of hard exclusive processes as compared to elastic hadron–hadron scattering [21], see Sec. 4.

For transversely polarized virtual photons the space–time picture of the interaction is more complicated than in the longitudinal case. Owing to the different spin structure of the $\gamma_T^* \rightarrow q\bar{q}$ vertex, configurations of very different size — from hadronic size to $1/Q$ — contribute to the interaction. The hadronic size configurations correspond to $z \sim 1$ or 0, and $k_\perp \sim \Lambda_{\text{QCD}}$. They

¹There is an approach to high–energy scattering in which the projectile particle is represented as a superposition of eigenstates of the scattering matrix, see *e.g.* Ref. [18] and references therein. Equation (8) implies that states with different transverse size, d , should be orthogonal. However, the extension of Eq. 8 to the case of elastic scattering indicates that transitions between configurations with different d are allowed for finite t . This suggests that the eigenstate model should be a reasonable approximation only for small values of t .

are dual to two jets aligned along the virtual photon direction and are referred to as aligned jet configurations. They are expected to interact with the target with typical hadronic cross sections, giving the dominant contribution to the structure function F_2 at $Q^2 \sim \text{few GeV}^2$ and $x \sim 10^{-2}$, see Sec. 3.2. Also, such configurations can easily scatter elastically from the target, and thus are an important source of diffractive scattering, see Sec. 5.

3 Inclusive γ^*p scattering at small x

3.1 DGLAP evolution and the HERA data

We start our discussion of γ^*p scattering at high energies with inclusive DIS. Inclusive DIS is the main source of information about the parton distributions in the nucleon at small x . Because of the relatively simple structure of QCD factorization, it is also the main testing ground for higher-order QCD calculations and resummation approaches.

The validity of QCD factorization and DGLAP evolution for inclusive DIS have extensively been tested in fixed-target experiments, probing the quark/antiquark densities in the nucleon at values $x > 10^{-2}$ see *e.g.* Ref. [22] for a review. Going to smaller x , DGLAP evolution produces a fast increase of the parton densities, related to the fact that the gluon has spin 1 [8, 9], which implies a fast increase of the DIS cross section with energy. This prediction has spectacularly been confirmed by the measurements with the HERA ep collider. Fig. 4 shows a summary of the F_2 proton structure function data taken by H1 and ZEUS compared to a QCD fit based on NLO DGLAP evolution [23]. The data clearly support the interrelation of the x - and Q^2 -dependence as predicted by DGLAP evolution. The analysis of the data found that effects of next-to-next-to-leading order (NNLO) terms of the form of α_s^2 multiplied by a function of $\alpha_s \ln(Q^2/Q_0^2)$ generally appear to be small. It is remarkable that the DGLAP approximation, which does not account for all potentially large terms containing $\ln(1/x)$, describes the presently available high-energy data so well.

More detailed insights into the “workings” of the DGLAP approximation can be gained by studying the effective power behavior in x of the structure function and the individual parton distributions in the NLO fit,

$$F_2 \propto x^{-\lambda_2}, \quad xG(x) \propto x^{-\lambda_g}, \quad \sum_f e_f^2 x\bar{q}_f(x) \propto x^{-\lambda_q} \quad (x < 10^{-2}), \quad (10)$$

where the exponents depend on Q^2 , see Fig. 5. At low Q^2 , $\lambda_2 \approx 0.1$, reflecting the energy dependence expected for the cross section of soft hadronic processes. Starting from $Q^2 \approx 0.5 \text{ GeV}^2$ λ_2 grows, reaching a value of ~ 0.4 at $Q^2 \sim 10 \text{ GeV}^2$ (A.Levy, private communication). For $Q^2 > 3 \text{ GeV}^2$, one observes that $\lambda_g \approx \lambda_2$, indicating that in this Q^2 -region the x -dependence of the structure function is indeed driven by the gluon distribution. For lower Q^2 , however, λ_g is significantly different from λ_2 , becoming even negative at $Q^2 \approx 2 \text{ GeV}^2$. Thus, while the NLO DGLAP approximation formally describes the x -dependence of the structure function even at low Q^2 , the price to be paid is the lack of a smooth matching of the x -dependence of the gluon distribution to the soft regime. This may indicate the presence of significant corrections to the

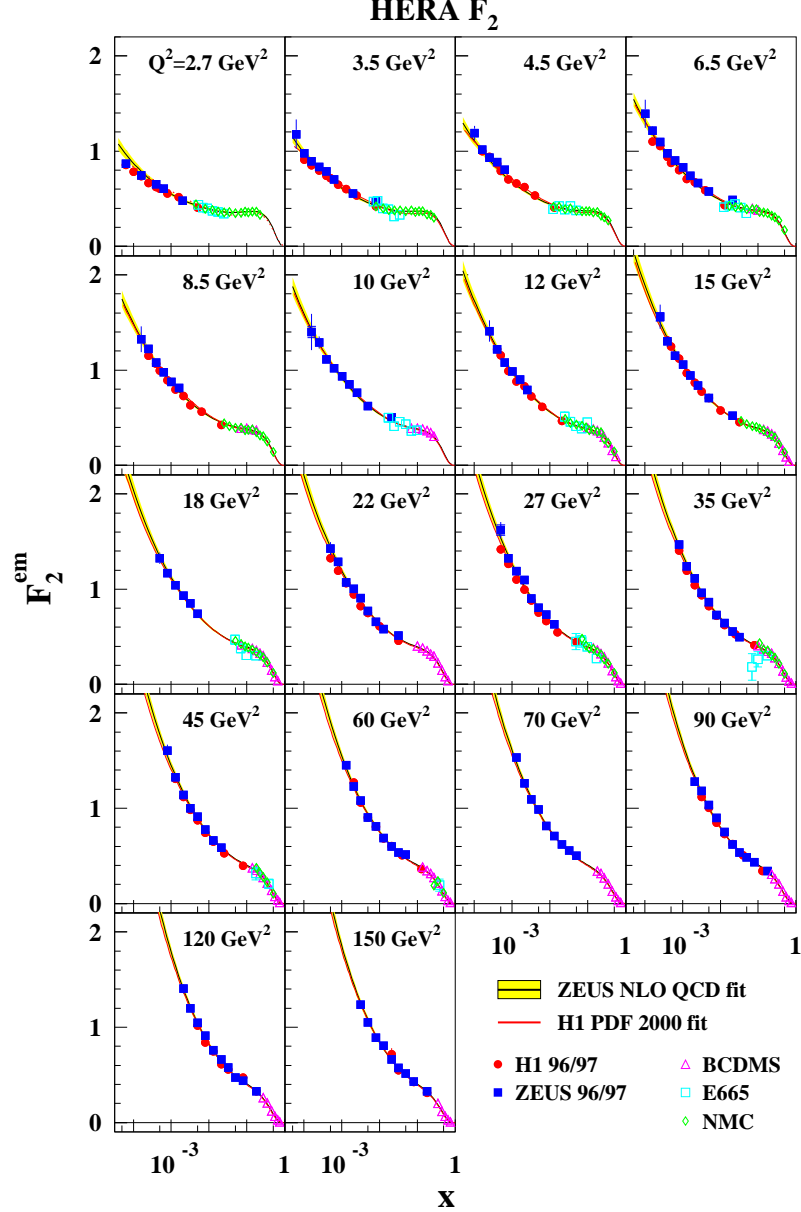


Figure 4: The proton structure function, $F_2(x)$, as measured by the H1 and ZEUS experiments at HERA [23]. Also included are data from fixed-target experiments. The lines show a QCD fit based on the NLO DGLAP approximation.

leading-twist description of DIS at small x for $Q^2 \leq 3 \text{ GeV}^2$. The dynamical origin of these corrections will be discussed in Sec. 3.2.

The data show that the deviation from the soft energy dependence of F_2 starts at surprisingly low scales, $Q^2 \ll 1 \text{ GeV}^2$. Within the DGLAP approximation this behavior can be explained by the presence of a large non-perturbative gluon density in the nucleon at moderate x at a low scale [24]. This is principally consistent with the idea of spontaneous chiral symmetry breaking, according to which most of the nucleon mass resides in gluon fields.

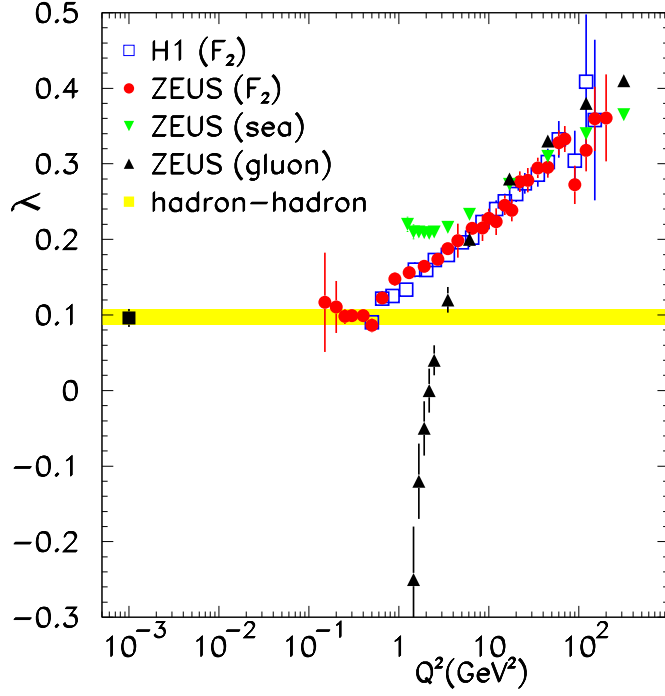


Figure 5: The exponents characterizing the x -dependence of F_2 , λ_2 , the gluon distribution, λ_g (black squares), and the sea quark distributions, λ_q (green triangles), *cf.* Eq. (10), as extracted from the NLO DGLAP fit to the H1 and ZEUS data (A.Levy, private communication).

3.2 Space–time picture of inclusive DIS

Many of the observed features of inclusive DIS at small x can be understood within the space–time picture in the target rest frame, *cf.* Sec. 2.2. In this formulation, corrections to the leading–twist approximation at low Q^2 appear because of the contribution from large dipole sizes. This allows us to quantify the region of validity of the leading–twist approximation, and develop an “interpolating” approximation valid in a wide range of Q^2 .

Following the logic outlined in Sec. 2.2, one can express the total γ^*p cross section at small x as a superposition of $q\bar{q}$ dipole cross sections, characterized by the longitudinal momentum fraction of the quark, z , and the dipole size, d :

$$\sigma_{L,T}(x, Q^2) = \int_0^1 dz \int d^2d \sigma^{q\bar{q}\text{-hadron}}(z, d, x) |\psi_{L,T}^\gamma(z, d, Q^2)|^2, \quad (11)$$

where $\psi_{L,T}^\gamma(z, d)$ denotes the light–cone wave function of the $q\bar{q}$ component of the virtual photon, calculable in quantum electrodynamics. An important question is which dipole sizes dominate in the integral. For a longitudinally polarized photon, the modulus squared of the wave function is given by

$$|\psi_L^\gamma(z, d, Q^2)|^2 = \frac{6\alpha_{\text{em}}Q^2}{\pi^2} \sum_{f=1}^{N_f} e_f^2 [z(1-z)K_0(\epsilon d)]^2, \quad (12)$$

where K_0 is the modified Bessel function and $\epsilon^2 = z(1-z)Q^2 + m_f^2$ [25]. One can verify by direct calculation that in this case the contributions from large dipole sizes are suppressed at large Q^2 , if the integral (11) is evaluated with the LO expression for the dipole–nucleon cross section, Eq. (8) [21]. In fact, Eqs. (11, 12) and (8) are formally equivalent to the LO DGLAP approximation in QCD, *cf.* the discussion below. The effective scale in the gluon distribution entering the dipole cross section can be determined by comparing (11) with the LO DGLAP expression; one finds $Q_{\text{eff}}^2 \approx 9/d^2$ for HERA kinematics [26]. Note that the factor $xG(x, Q_{\text{eff}}^2)$ in Eq. (8) results in a fast increase of the cross section with energy, in contrast to the two–gluon exchange model of Refs. [27, 28, 29], where the cross section is energy–independent.

When applying Eq. (11) to transversely polarized photons, the distribution of dipole sizes is significantly wider than in the longitudinal case. At $Q^2 \sim \text{few GeV}^2$, the transverse cross section receives sizable contributions from dipole sizes for which the perturbative approximation for the dipole–nucleon cross section, *cf.* Eq. (8), becomes invalid. Still, at large Q^2 the perturbative contribution should dominate, because of the faster increase with energy of the parton distribution for the smaller–size quark–gluon configuration. The contribution from large–size $q\bar{q}$ configurations is strongly suppressed by Sudakov form factors; it is actually represented by large–size $q\bar{q}g, \dots$ configurations.

Equation (11) can serve as the basis for an “interpolating” model that describes γ^*p interactions over a wide range of Q^2 for both transverse and longitudinal polarizations [30]. There is ample evidence — *e.g.* from studies of γN and πN elastic scattering — that real photons in high–energy reactions have transverse sizes comparable to pions. A way to ensure this within the $q\bar{q}$ dipole description is to introduce a dynamical quark mass of $\sim 300 \text{ MeV}$, which is consistent with the phenomenology of spontaneous chiral symmetry breaking [31]. The cross section for the scattering of such a “hadronic–size” dipole with the target can then be inferred from the πN scattering data. For small dipoles, $d \leq 0.4 \text{ fm}$, the cross section can be calculated perturbatively. When evaluating the leading–twist expression, it is important to accurately treat the kinematic limits of the integral over the gluon momentum fractions, as this leads to an additional dependence of the dipole cross section on Q^2 . A dipole cross section obtained by matching the two prescriptions is shown in Fig. 6. This function is then averaged with the photon wave function for massive quarks, *cf.* Eq. (11). This model reproduces well the HERA F_{2p} data for $Q^2 \geq 0.1 \text{ GeV}^2$, and correctly predicts σ_L [30].

In order to make contact with the analysis of Sec. 3.1, we need to state more precisely how the dipole picture is related to the DGLAP approximation in QCD. In LO, it has been demonstrated explicitly that Eqs. (8) and (11) can be obtained by rewriting the LO DGLAP expression for the γ^*p cross section [17]. This simple relation appears because in the leading logarithmic approximation the separation of the process according to time in the target rest frame — transition of the virtual photon into a $q\bar{q}$ pair (photon wave function), and interaction of the pair with the target (dipole cross section) — coincides with the separation of transverse momenta in $k_{\perp}^2 \sim Q^2$ and $k_{\perp}^2 \ll Q^2$ in the partonic ladder. Beyond the leading order, one needs to explicitly include $q\bar{q}g$ component of the photon wave function, and the distinction between the wave function and the dipole interaction with the target becomes more delicate. Although in principle the leading–twist dipole picture should be equivalent to the DGLAP approximation in any order of the expansion, in practice the problem of formulating a consistent dipole picture in NLO has not been solved yet. Also, it is worth emphasizing that the correspondence between parton distributions and amplitudes of physical processes is not always direct. In particular, the

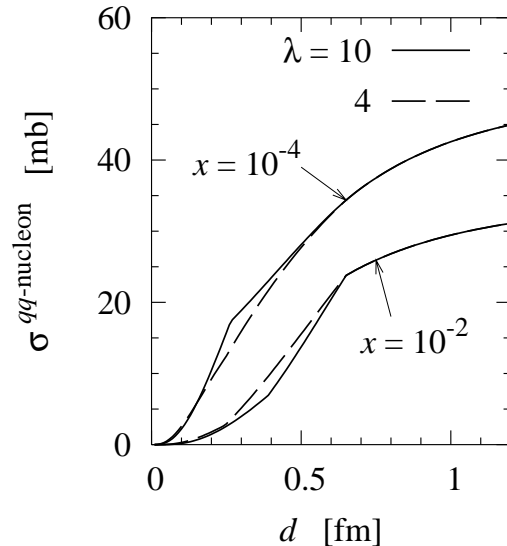


Figure 6: The dipole–nucleon cross section in the “interpolating” model of Ref. [30]. Shown are the results corresponding to two different values of the parameter, λ , determining the effective scale, Q_{eff}^2 .

parton model–type contribution, which naturally leads to diffractive processes, is hidden in the boundary condition for the QCD evolution of the parton distributions.

In spite of the lack of an explicit NLO analysis in the dipole picture, it still seems to be of relevance that the region of Q^2 where the NLO DGLAP analysis leads to a gluon exponent λ_g dropping below the soft value (see Fig. 5) corresponds in the dipole model to contributions from $d > 0.4$ fm, where nonperturbative effects become important. Thus, it seems that the “anomalous” behavior of λ_g is a consequence of the leading–twist DGLAP approximation trying to mock up higher–twist corrections at low Q^2 . The dipole picture allows us to quantify the region of applicability of the leading–twist approximation at low Q^2 , and suggests a natural way to incorporate non-perturbative effects.

Equations (8) and (11) are valid also within the leading $\alpha_s \ln(x_0/x)$ approximation. Furthermore, they can be derived from the eikonal model expression for the propagation of a heavy quarkonium through a hadronic medium [32].

3.3 Breakdown of the DGLAP approximation at very small x

The observation of the fast increase of parton densities at small x has stimulated theoretical discussions of the stability of the DGLAP approximation at small x . In fact, in the kinematic limit of fixed Q^2 and $x \rightarrow 0$ the effective parameter of the perturbative QCD expansion is multiplied by a factor $\ln(x_0/x)$, which arises due to gluon emission in multi–Regge kinematics (rapidity distance between adjacent gluons $\gg 2$), and the hierarchy of dominant terms is changed as compared to the DGLAP approximation. The constant x_0 is determined by the typical momentum fraction in the initial parton distributions; usually $x_0 \sim 0.1$.

A simple kinematic estimate shows that in typical HERA kinematics the DGLAP approximation is still reliable. The rapidity span at HERA is approximately $\ln(Q/xm_N) \approx 10$ for $x = 10^{-4}$ and $Q = 2.5 \text{ GeV}$. To obtain a significant $\ln(x_0/x)$ term, the distance in rapidity between adjacent partons in the ladder should be $\gg 2$. Thus, the number of radiated gluons in multi-Regge kinematics at HERA is $\ll (10 - 4)/2 - 1 \approx 2$, where we took into account that each of the fragmentation regions occupies at least two units in rapidity. This simple estimate agrees well with a numerical study of NLO QCD evolution, which indicates that the average change of x in the HERA region does not exceed 10, corresponding to $\Delta y = \ln(x_0/x) \approx 2$, provided that $Q_0^2 \geq 1 \text{ GeV}^2$ [33]. Since one (two) logarithms of x are effectively taken into account by the NLO (NNLO) approximation, there is no need for a special treatment of $\ln(x_0/x)$ effects at HERA kinematics. A similar estimate shows that at LHC kinematics the radiation of 5–6 gluons is permitted. Thus, at LHC energies and above the resummation of $\ln(x_0/x)$ terms becomes a practical issue.

The program of resumming leading $\alpha_{\text{em}} \ln(x_0/x)$ terms started in quantum electrodynamics [20]. In QCD, the reggeization of gluons slows down the energy dependence of amplitudes of high-energy processes [34, 35].² In the leading $\alpha_s \ln(x_0/x)$ approximation (Balitsky–Fadin–Kuraev–Lipatov, or BFKL, approximation) [36], where energy–momentum conservation and the running of the coupling constant are neglected, the reggeization of gluons is canceled by contributions from multigluon radiation. NLO corrections to a large extent subtract kinematically forbidden contributions, leading to a large negative contribution to the structure functions [37, 38]. Another feature of this approach is the lack of an unambiguous separation between perturbative and nonperturbative QCD effects [37]. Thus, this approximation seems to be limited to the description of single-scale hard processes where DGLAP evolution is unimportant in a wide kinematic range, such as $\gamma^*(Q^2) + \gamma^*(Q^2) \rightarrow \text{hadrons}$, or two-body processes where the hardness is controlled by proper choice of final state like, such as $\gamma^* + \gamma^* \rightarrow \Upsilon\Upsilon$.

The resummation approaches of Refs. [39, 40] predict a significantly slower increase of amplitudes with energy than the LO BFKL approximation, and possibly even oscillations in the energy dependence. Most of the reduction is due to the better account of energy–momentum conservation in these approaches, and account of the running of the coupling constant. At extremely small x (beyond the reach of LHC) much of the LO BFKL results reappear, but with a slower dependence on x . For the parton densities in the nucleon, where $x_0 \approx 0.1$ is a reasonable value for the constant in the $\ln(x_0/x)$ factor, resummation effects should be small for $x \geq 10^{-4}$, that is, for the whole HERA range above $Q^2 \geq 2 \text{ GeV}^2$. At smaller x , the result of the resummed evolution is close to that of NLO DGLAP evolution down to $x \sim 10^{-6}$, but differs strongly from NNLO [41]. This suggests that NLO DGLAP evolution could be a good guess for the parton densities down to the very small x values probed at LHC, even though the underlying dynamics may change significantly at $x \leq 10^{-4}$.

²The high-energy behavior of two-body amplitudes with color-octet quantum numbers in the crossed channel in QCD is given by the Regge pole formula, $(1/x)^{\beta(t)}$, where $\beta(t)$ decreases with increase of $-t$. In leading order of α_s QCD gives $\beta(t) = 1$. Thus, gluons in QCD (as well as quarks) are reggeons.

4 Exclusive processes in γ^*p scattering at small x

4.1 QCD factorization for hard exclusive processes

The concept of QCD factorization can be extended to certain exclusive channels in γ^*p scattering, namely processes of the type

$$\gamma_L^*(q) + N(p) \rightarrow \text{“Meson”}(q + \Delta) + \text{“Baryon”}(p - \Delta), \quad (13)$$

at large virtuality, $Q^2 \equiv -q^2$, and center-of-mass energy, $W^2 \equiv (p + q)^2$, with fixed $x = Q^2/(W^2 + Q^2)$, and fixed small invariant momentum transfer, $t \equiv \Delta^2$. Examples include the production of light vector mesons (ρ, ρ') [21], heavy vector mesons ($J/\psi, \psi', \Upsilon$) [21], and real photons (deeply-virtual Compton scattering, DVCS) [42, 43, 44, 45, 46, 47, 48]. Closely related to these processes are certain hadron-induced reactions, such as the diffractive dissociation of pions, $\pi + T \rightarrow 2 \text{ jets} + T$, where T denotes a hadronic target (nucleon or nucleus) [16]. These exclusive processes probe the interaction of small-size color singlets with hadronic matter in much more detail than inclusive DIS. They also provide new information about the transverse spatial structure of the nucleon, contained in the so-called generalized parton distributions.

The basis for the analysis of exclusive processes (13) is the QCD factorization theorem [49], which extends the initial analysis of Ref. [21] for the small- x limit. It states that the amplitude can be represented as a convolution of three functions, as depicted in Fig. 7:

$$A^{\gamma_L^* N \rightarrow M+B} = \sum_{i,j} \int_0^1 dz \int dx_1 f_{i/p}(x_1, x - x_1, t; \mu) H_{ij}(x_1, x, z, Q^2; \mu) \phi_j^M(z, \mu) + \text{power corrections}. \quad (14)$$

Here, f is the generalized parton distribution (GPD), which describes the amplitude for the nucleon to “emit” and “absorb” a parton with longitudinal momentum fractions x_1 and $x_2 =$

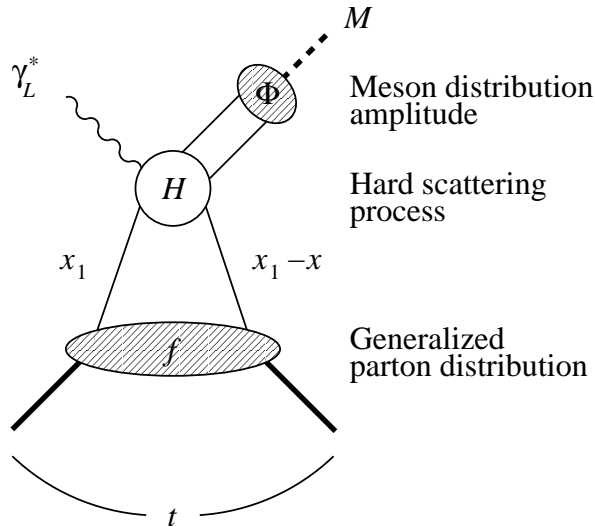


Figure 7: Factorization of the amplitude of hard exclusive meson production, Eq. (14).

$x_1 - x$, respectively, accompanied by an invariant momentum transfer, t , and, possibly, a transition to another baryonic state. At zero momentum transfer, $x_1 = x_2$ and $t = 0$, the GPD's coincide with the usual parton densities measured in inclusive DIS. (For a review of the properties of GPD's and their applications, see Refs.[50, 51].) Furthermore, ϕ^M is the distribution amplitude describing the conversion of a $q\bar{q}$ pair with relative longitudinal momentum fraction z to the produced meson (or photon). Finally, H_{ij} denotes the amplitude of the hard partonic scattering process, which is calculable in powers of $\alpha_s(Q^2)$. The indices i, j label the different parton species. The contribution of diagrams in which the hard scattering process involves more than the minimum number of partons is suppressed by $1/Q^2$. An important consequence of factorization is that the t -dependence of the amplitude rests entirely in the GPD. Thus, different processes probing the same GPD should exhibit the same t -dependence.

4.2 Space–time picture of hard exclusive processes

The physics of hard exclusive processes at small x becomes most transparent when following the space–time evolution in the target rest frame. As in the case of inclusive scattering, this approach allows one to expose the limits of the leading–twist approximation, and to quantify power corrections due to the finite transverse size of the produced meson.

In exclusive vector meson production, $\gamma_L^* N \rightarrow VN$, one can identify three distinct stages in the time evolution in the target rest frame. The virtual photon dissociates into a $q\bar{q}$ dipole of transverse size $d \sim 1/Q$ at a time $\tau_i = l_{\text{coh}}/c \approx 1/(m_N x)$ before interacting with the target, *cf.* Eq. (5). The $q\bar{q}$ dipole then scatters from the target, and “lives” for a time $\tau_f \gg \tau_i$ before forming the final state vector meson. The difference in the time scales is due to the smaller transverse momenta (virtualities) allowed by the meson wave function as compared to the virtual photon.

In the leading logarithmic approximation in $\ln(Q^2/\Lambda_{\text{QCD}}^2)$, the effects of QCD radiation can again be absorbed in the amplitude for the scattering of the small–size dipole off the target. It can be shown by direct calculation of Feynman diagrams that the leading term for small dipole sizes is proportional to the generalized gluon distribution, $G(x_1, x_2, t; Q_{\text{eff}}^2)$, where $Q_{\text{eff}}^2 \propto d^{-2}$ [17]. A simpler approach is to infer the result for the imaginary part of the amplitude from the expression for the cross section, Eq. (8), via the optical theorem. The imaginary part is proportional to the generalized gluon distribution at $x_1 = x$ and $x_2 = 0$. At sufficiently large Q^2 , the generalized gluon distribution at small x_1 and x_2 can be calculated by perturbative evolution, starting from the “diagonal” generalized gluon distribution, $x_1 = x_2 \gg x$, at a low scale [52, 53, 54]. In applications to vector meson production at HERA, where the effective scale is of the order $Q_{\text{eff}}^2 \sim \text{few GeV}^2$, the “skewness” effects induced by the evolution are not very substantial, and one may approximate the generalized gluon distribution by the diagonal one at the scale Q_{eff}^2 . It is convenient to separate the t -dependence and write the diagonal generalized gluon distribution in the form

$$G(x, x, t; Q_{\text{eff}}^2) = G(x, Q_{\text{eff}}^2) F_g(x, t; Q_{\text{eff}}^2), \quad (15)$$

where $G(x, Q_{\text{eff}}^2)$ is the usual gluon density and F_g is the “two–gluon form factor” of the target, which satisfies $F_g(x, t = 0; Q_{\text{eff}}^2) = 1$. Altogether, one obtains for the dipole–hadron scattering

amplitude in this approximation

$$A^{q\bar{q}-N}(x, d^2, t) = 2\pi i F^2 W^2 d^2 \alpha_s(Q_{\text{eff}}^2) xG(x, t, Q_{\text{eff}}^2) F_g(x, t, Q_{\text{eff}}^2). \quad (16)$$

The amplitude for the hadronic process (13) is then given by the convolution of Eq. (16) with the light-cone wave function of the virtual photon, Eq. (12), and that of the produced vector meson, ψ^V . In coordinate representation,

$$A^{\gamma^* N \rightarrow V N} = \int_0^1 dz \int d^2 d \psi_L^\gamma(z, d) A^{q\bar{q}-N}(x, d^2, t) \psi^V(z, d), \quad (17)$$

where the integration is over the quark longitudinal momentum fraction, z , and the transverse dipole size, d .

In Eq. (17), the wave function of the vector meson of transverse size $1/m_V$ is convoluted with the wave function of the virtual photon of significantly smaller transverse size, $1/Q$. One may say that the meson in this process is “squeezed”, *i.e.*, forced to couple in a configuration much smaller than its natural hadronic size. In the leading-twist approximation one neglects the spatial variation of the vector meson wave function and substitutes it by the distribution amplitude,

$$\psi^V(z, d) \rightarrow \psi^V(z, 0) \equiv \phi^V(z) \quad (18)$$

(in momentum representation, the distribution amplitude is the integral of the wave function over transverse momenta). The integral over transverse sizes can then be performed explicitly, using Eqs. (12) and (16). After restoring the real part of the amplitude using its analyticity properties, the differential cross section is obtained as [21]

$$\begin{aligned} \frac{d\sigma_L^{\gamma^* N \rightarrow V N}}{dt} &= \frac{3\pi^3 \Gamma_V m_V \eta_V^2}{N_c^2 \alpha_{\text{em}} Q^6} \\ &\times \alpha_s^2(Q_{\text{eff}}^2) \left| \left(1 + \frac{i\pi}{2} \frac{d}{d \ln x} \right) xG(x; Q_{\text{eff}}^2) \right|^2 F_g^2(x, t; Q_{\text{eff}}^2). \end{aligned} \quad (19)$$

Here, Γ_V is the leptonic width of the vector meson, which defines the normalization of the meson wave function, and

$$\eta_V \equiv \frac{1}{2} \int_0^1 dz \frac{\phi^V(z)}{z(1-z)} \Big/ \int_0^1 dz \phi^V(z); \quad (20)$$

$\eta_V \rightarrow 1$ at asymptotically large Q^2 . These expressions apply to production by a longitudinally polarized photon. For transverse polarization, the nonperturbative contribution is suppressed only by a Sudakov-type form factor, similar to the case of $F_2(x, Q^2)$ in inclusive $\gamma^* p$ scattering. This contribution originates from highly asymmetric $q\bar{q}$ pairs ($z \sim 0$ or 1) in the γ_T^* wave function, which have transverse size similar to that of hadrons. We note that elastic photo/electroproduction of J/ψ mesons has been evaluated also within the LO BFKL approximation [55]. The function $xG(x, Q^2)$ that enters there has no relation to the conventional DGLAP gluon distribution, which is defined within the DGLAP approximation only.

Equation (19) is based on the leading logarithmic approximation in $\ln(Q^2/\Lambda_{\text{QCD}}^2)$, as well as on the leading-twist approximation, Eq. (18). While it already exhibits many qualitative

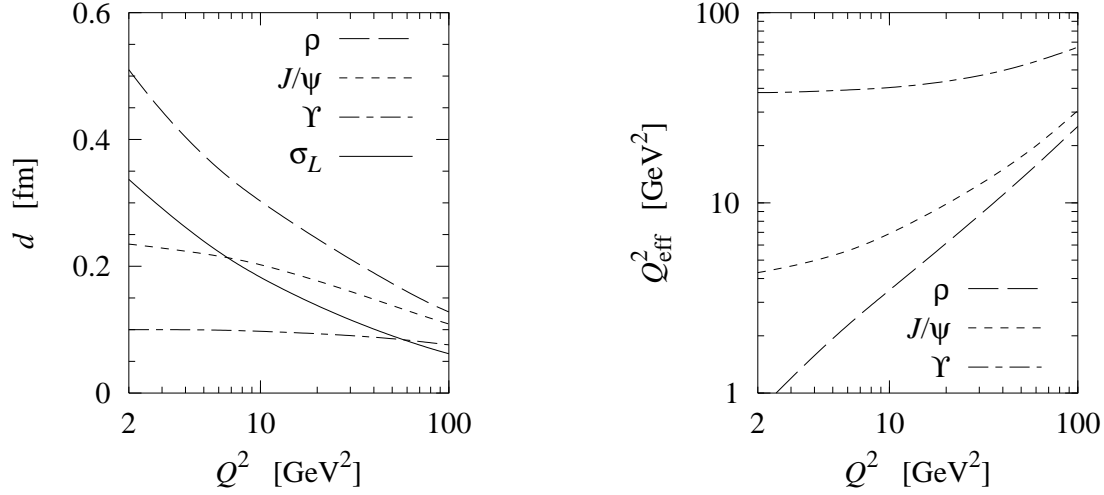


Figure 8: The average dipole size, d , (left) and the effective scale, Q_{eff}^2 , (right) in exclusive vector meson production (ρ , J/ψ , Υ) by longitudinally polarized photons, as a function of Q^2 [26, 56]. Also shown are the average values of d in the integrand of the expression for the inclusive cross section, σ_L .

features seen in the data (see below), two important effects need to be taken into account before a quantitative comparison can be attempted. First, because the wave function of the vector meson in Eq. (17) is significantly broader than that of the γ_L^* , the effective dipole sizes in the meson production amplitude, Eq. (16), are substantially larger than in σ_L , Eq. (11), see Fig. 8. As a result, the effective scale in the gluon distribution, Q_{eff}^2 , is smaller in vector meson production than in σ_L , see Fig. 8 [26, 56]. This effect slows the x - (energy) dependence of the cross section compared to the naive estimate, $Q_{\text{eff}}^2 = Q^2$. Second, numerical studies using model wave functions show that retaining the full d -dependence of the vector meson wave function in the convolution integral (17) results in a substantial decrease of the absolute cross section at moderate Q^2 as compared to the leading-twist approximation, Eq. (18), as well as in a slower Q^2 dependence [26, 56]. These higher-twist effects, related to the finite size of the vector meson, limit the region of validity of the leading-twist approximation (18) and need to be taken into account in quantitative estimates at low Q^2 .

4.3 Vector meson production at HERA

With proper choice of the effective scale, Q_{eff}^2 , and inclusion of higher-twist effects due to the finite transverse size of the meson, one can quantitatively compare the results of the leading logarithmic approximation, Eqs. (16) and (17), with the HERA data on heavy and light vector meson production. The data confirm in particular the following predictions of this picture:

- *Increase of cross section with energy.* Equation (19) implies that $d\sigma/dt(t=0)$ grows with energy as $[xG(x, Q_{\text{eff}}^2)]^2$, with Q_{eff}^2 estimated to be $\sim 3 \text{ GeV}^2$. When combined with the LO gluon density obtained from fits to DIS data, this implies a growth $\propto W^{0.8}$. Such

behavior has been observed for ρ production at $Q^2 = 10 - 20 \text{ GeV}^2$, and for J/ψ production starting from $Q^2 = 0$ [57]. The later onset of the hard regime for ρ electroproduction is due to the rather slow “squeezing” of the $q\bar{q}$ configuration in the ρ meson; it reaches a size comparable to that of the J/ψ only at $Q^2 \sim 20 \text{ GeV}^2$, see Fig. 8.³ The naive choice $Q_{\text{eff}}^2 = Q^2$ would imply a too fast growth, *cf.* Fig. 5. For soft interactions, on the other hand, $d\sigma/dt(t=0) \propto W^{0.32}$, and the growth is even smaller for the cross section integrated over t .

- *Decrease of cross section with Q^2 .* The decrease with Q^2 of σ_L for ρ -meson production, and of the total cross section for J/ψ production, is slower than $1/Q^6$, due to the Q^2 -dependence of $\alpha_s G$ in Eq. (19), as well as finite-size (higher-twist) effects. This is best observed in J/ψ electroproduction, where the model of Ref. [55], which neglects finite-size effects, predicts a decrease of the cross section by a factor of ~ 5 faster than observed in the kinematic region covered by the H1 experiment.
- *Absolute cross sections.* The absolute cross sections for vector meson production are well reproduced, provided that higher-twist effects due to the finite size of the vector meson are taken into account [26, 56].
- *Dominance of longitudinal cross section.* The data on ρ production indicate $\sigma_L \gg \sigma_T$ for $Q^2 \gg m_V^2$, in agreement with our picture.
- *Universality of t -dependence.* Comparison of ρ and J/ψ electroproduction data clearly show the universality of the t -dependence at large Q^2 , where the vector mesons are “squeezed”, and the t -dependence originates solely from the two-gluon form factor, see Fig. 9.
- *Flavor symmetry.* Since the interaction of the $q\bar{q}$ dipole with the gluon distribution is flavor blind, one expects the restoration of $SU(3)$ flavor symmetry in vector meson production for $Q^2 \gg m_V^2$. For example, $\phi : \rho = (2 : 9)$ in the flavor symmetry limit. The violation of $SU(3)$ flavor symmetry due to increase of the wave function of the vector meson at small distances with increasing quark mass leads to an enhancement of this ratio by a factor ~ 1.2 .

A new situation is encountered in the photoproduction of Υ mesons. In this case, the approximation of the generalized gluon distribution by the usual gluon density becomes invalid (large “skewness” and large Q_{eff}^2), and the real part of the amplitude becomes significant. Together, these effects increase the predicted cross section by a factor of about 4 [59, 60]. For Υ production $Q_{\text{eff}}^2 \approx 40 \text{ GeV}^2$, leading to an energy dependence of the cross section as $d\sigma/dt(t=0) \propto W^{1.7}$.

Closely related to vector meson production is the production of real photons (deeply virtual Compton scattering, DVCS). This process has been the subject of intense theoretical study in the region of moderate x , accessible in fixed-target experiments (HERMES at DESY, COMPASS

³In the case of the ρ -meson production initiated by the transverse photon, the squeezing is generated by the Sudakov form factor as well as by the more rapid increase with energy of the small size contribution. The observed behavior of σ_L/σ_T can be fitted within the current models [58].

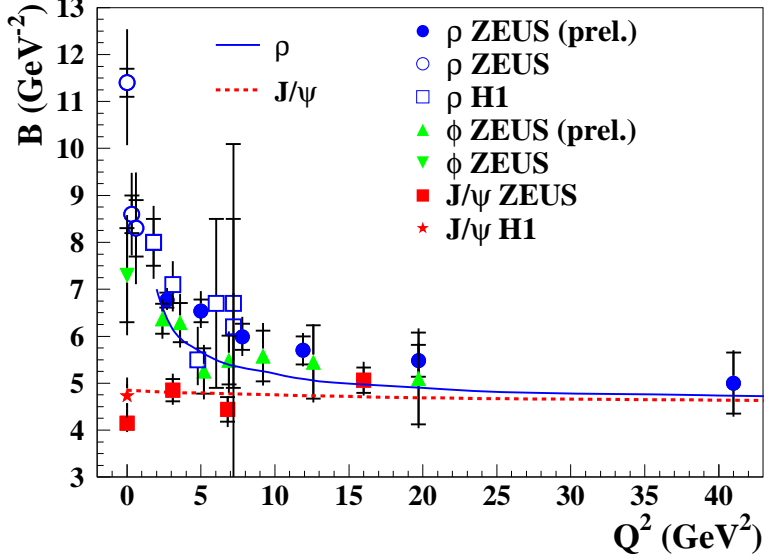


Figure 9: The HERA H1 and ZEUS data for the t -slopes of the differential cross sections for the exclusive electroproduction of ρ , ϕ and J/ψ mesons, as a function of Q^2 . The convergence of the different slopes at large Q^2 indicates the dominance of small-size configurations in the production process (“squeezing”). The solid line shows the Q^2 -dependence obtained in the calculation of Ref. [26]. The data are from Ref. [57].

at CERN, Jefferson Lab), and is considered the main tool for probing the generalized quark distributions in the nucleon [61, 43, 45, 46]. At small x , the DVCS amplitude has been computed in the leading $\ln(Q^2/\Lambda_{\text{QCD}}^2)$ approximation outlined in Sec. 4.2, and found to be substantially enhanced as compared to the forward amplitude, $\gamma^*p \rightarrow \gamma^*p$ [47]. The DVCS cross section reported by the HERA experiments is in reasonable agreement with these predictions, as well as with the color dipole model of Ref. [62]; see Ref. [63] and references therein. The HERA data at small x are also well described by an NLO QCD analysis [64, 65], in which the modeling of the input GPD’s is a much more challenging problem than in LO, see Ref. [65] for details. DVCS at small x and the closely related process of production of Z -bosons, $\gamma + p \rightarrow Z + p$, were also studied within the leading $\alpha_s \ln(x_0/x)$ approximation [42].

To summarize, the HERA data on exclusive electroproduction of vector mesons clearly show the transition to the perturbative QCD regime for $Q^2 \geq 10 - 20 \text{ GeV}^2$. This conclusion is consistent with the observation of color transparency phenomena in several other processes. It establishes the study of exclusive processes (x , Q^2 and t -dependence of the cross section) as a way to extract detailed information about the interaction of small dipoles with hadrons, as well as about the generalized parton distribution in the nucleon.

4.4 Transverse spatial distribution of gluons in the nucleon

An important aspect of hard exclusive processes at small x is that they provide information about the transverse spatial distribution of gluons in the nucleon. It is contained in the Fourier

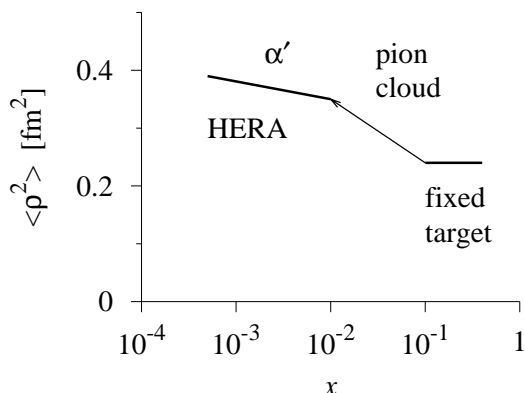


Figure 10: The average squared transverse radius of the gluon distribution in the nucleon, $\langle \rho^2 \rangle = \int d^2 \rho \rho^2 F_g(x, \rho; Q_{\text{eff}}^2)$, as a function of x , as extracted from J/ψ photoproduction data ($Q_{\text{eff}}^2 = 3 \text{ GeV}^2$) at various energies.

transform of the two-gluon form factor, Eq. (15),

$$F_g(x, \rho; Q_{\text{eff}}^2) \equiv \int \frac{d^2 \Delta_{\perp}}{(2\pi)^2} e^{i(\Delta_{\perp} \rho)} F_g(x, t = -\Delta_{\perp}^2; Q_{\text{eff}}^2), \quad (21)$$

where ρ is a transverse coordinate variable. The function $F_g(x, \rho; Q_{\text{eff}}^2)$ is positive definite [66] and describes the spatial distribution of gluons in the transverse plane, $\int d^2 \rho F_g(x, \rho; Q_{\text{eff}}^2) = 1$.

The convergence of the t -slopes of ρ and J/ψ production at large Q^2 (see Fig. 9) demonstrates that the t -dependence of the differential cross section is dominated by the two-gluon form factor. The two-gluon form factor can thus be extracted from the J/ψ photoproduction data ($Q_{\text{eff}}^2 \approx 3 \text{ GeV}^2$), with small corrections ($\sim 10\%$) due to the finite transverse size of the J/ψ meson. This process has been measured over a wide range of energies; see Refs. [67, 68] for an overview of the data. At fixed-target energies, $x \sim 10^{-1}$, the t -dependence of the data is well described by a two-gluon form factor of dipole form,

$$F_g = (1 - t/m_g^2)^{-2}, \quad m_g^2 = 1.1 \text{ GeV}^2 \quad (x \sim 10^{-1}), \quad (22)$$

where the parameter, m_g , is close to that in the dipole fit to the axial form factor of the nucleon. This corresponds to a narrow spatial distribution of gluons in the transverse plane, with an average transverse radius $\langle \rho^2 \rangle = 8/m_g^2 \approx 0.28 \text{ fm}^2$, see Fig. 10. At HERA energies, $x \sim 10^{-2} - 10^{-3}$, the average radius is larger, $\langle \rho^2 \rangle \approx 0.35 \text{ fm}^2$. It also exhibits a slow growth with $\ln(1/x)$, with a slope, α' , significantly smaller than the value for soft interactions. The J/ψ photoproduction data from H1 give $\alpha'_{\text{hard}} = 0.08 \pm 0.17 \text{ GeV}^{-2}$ [69], the ZEUS electroproduction data $\alpha'_{\text{hard}} = 0.07 \pm 0.05(\text{stat})_{-0.04}^{+0.03}(\text{syst}) \text{ GeV}^{-2}$ [70], which should be compared to $\alpha' \approx 0.25 \text{ GeV}^{-2}$ for pp elastic scattering. This reflects the suppression of Gribov diffusion for partons with large virtualities, see the discussion in Sec. 2.2.

The change of the nucleon's average transverse radius between $x \sim 10^{-1}$ and 10^{-2} can naturally be explained by chiral dynamics. Pions in the nucleon wave function carry momentum fractions of the order m_{π}/m_N . For $x > m_{\pi}/m_N$ the pion cloud does not contribute to the gluon

distribution, and the two–gluon form factor is similar to the nucleon axial form factor, which also does not receive contributions from the pion cloud. For $x \ll m_\pi/m_N$, the pion cloud contributes to the gluon distribution and leads to an increase of $\langle\rho^2\rangle$ by 20 – 30%, see Fig. 10 [71].

It is worth emphasizing that for smaller x the increase of the transverse size should continue due to the Gribov diffusion. Indeed, a hard probe can interact with a parton of the soft ladder, responsible for the growth of the soft radius, if the soft parton’s momentum fraction is sufficiently small compared to x . At very small x and fixed Q^2 the rate of the growth should thus be comparable to that in the soft case [72]. No such effect is present in the BFKL model where the interaction of two small dipoles is considered.

The change of the transverse spatial distribution of gluons in the nucleon with the scale, Q_{eff}^2 , due to DGLAP evolution should generally be small [73]. For Q_{eff}^2 sufficiently large compared to the transverse spatial resolution, the parton decays happen essentially locally in transverse position. For fixed x , one finds that the transverse spatial distribution shrinks with increasing scale, because the distribution becomes sensitive to the input distribution (at the initial scale) at higher values of x , where it is concentrated at smaller transverse distances.

4.5 Color transparency in hard processes with nuclei

QCD predicts that the spatially small quark–gluon wave packets formed in hard γ^* –induced scattering processes interact weakly with hadronic matter, because of the color neutrality of the photon. At sufficiently small x , where the cross section is proportional to the gluon density, *cf.* Eq. (8), one expects the ratio of the cross sections for γ^* scattering from a nucleus and a single nucleon to be equal to the ratio of the respective gluon densities, a property known as generalized color transparency [16, 21]. Because with increasing Q^2 gluon shadowing at fixed x disappears (*cf.* the discussion in Sec. 5.4), one further expects that

$$\sigma_{\text{tot}}^{\gamma^*A}/(A\sigma_{\text{tot}}^{\gamma^*N}) \rightarrow 1 \quad (Q^2 \rightarrow \infty; x \text{ fixed, small}), \quad (23)$$

which is referred to as color transparency proper. Conversely, at fixed Q^2 and decreasing x , the ratio in Eq. (23) should decrease owing to the more important role of nuclear shadowing, and color transparency phenomena should completely disappear at very small x , where QCD factorization breaks down. This is in contrast to the two–gluon exchange model of Refs. [74, 75], which neglects the space–time evolution of the dipole. In this model nuclear shadowing is obtained from exchanges of additional gluon between the current and target fragmentation regions, which is a higher–twist effect ($\propto 1/Q^2$) and disappears at large Q^2 .

The color transparency phenomenon has been directly observed in three experiments:

- The total cross section for γ^*A scattering increases with the atomic number as A^α with $\alpha \approx 1$, faster than the cross section for a hadronic projectile, see Ref. [76] for a review of the experimental data.

- The cross section for coherent photoproduction of J/ψ mesons from nuclei increases with A much faster than that for coherent ρ meson production. The Fermilab E691 experiment [77] observed $\sigma^{\gamma^*+A \rightarrow J/\psi+A} \propto A^{1.46}$ at $E_\gamma = 150$ GeV. Color transparency predicts that the coherent cross section integrated over t is $\propto (A^2/R_A^2) \approx A^{4/3}$. This A -dependence corresponds to the coherent sum of collisions from independent nucleons without absorption. A somewhat faster A -dependence emerges because of the contribution of incoherent diffractive processes [19].
- The A -dependence of the cross section for coherent dijet production in pion-nucleus scattering is anomalously large, as predicted in Ref. [16]. The Fermilab E791 experiment [78] observed a dependence $\propto A^{1.54}$ at $E_\pi \approx 600$ GeV, similar to that in coherent J/ψ production. Note that the conventional Glauber approximation predicts $A^{1/3}$. Furthermore, the observed dependence of the cross section on the pion momentum fraction and the jet transverse momentum is well consistent with the perturbative QCD prediction of Ref. [19]. Notwithstanding the fact that the absolute cross section has not been measured, this is probably the first experimental observation of the high-momentum tail of the pion wave function as due to one-gluon exchange.

To summarize, there exists strong experimental evidence for color transparency in high-energy scattering. This phenomenon could be the basis for new “non-destructive” methods of investigating the microscopic structure of hadrons and nuclei in the future.

5 Diffraction in γ^*p scattering

5.1 QCD factorization for hard diffractive processes

Measurements of DIS at HERA have established the existence of a class of events in which the proton is observed in the final state, with a small invariant momentum transfer, t , and a hadronic system of invariant mass $M_X^2 \ll W^2$ is produced with a rapidity gap relative to the proton. In a frame in which the nucleon is fast-moving (*i.e.*, in parton model kinematics) such processes are characterized by the fractional energy loss of the proton, $x_P = (E_p^i - E_p^f)/E_p^i$, and the transverse momentum transfer, Δ_\perp , with $t = -(\Delta_\perp^2 + x_P^2 m_N^2)/(1 - x_P)$. In analogy with the corresponding phenomenon in hadronic collisions one refers to such processes as diffractive, although a priori the dynamics is not governed by soft physics.

Following suggestions of earlier works, a formal QCD factorization theorem was proved in Ref. [79, 80] for hard processes of the type

$$\gamma^* + p \rightarrow h + (\text{rapidity gap}) + X, \quad (24)$$

where X is either an inclusive state, or a state with extra hard activity (dijet production, heavy quark production, *etc.*), see Fig. 11. Similar to inclusive DIS, processes (24) with a given hadron h in the target fragmentation region are characterized by so-called conditional parton distribution functions, $f_j^h(\beta, Q^2, x_h, t)$, which are independent of the hard process and satisfy the same DGLAP evolution equations for fixed x_h and t . Here $\beta \equiv x/(1-x_h) = Q^2/(Q^2 + M_X^2)$

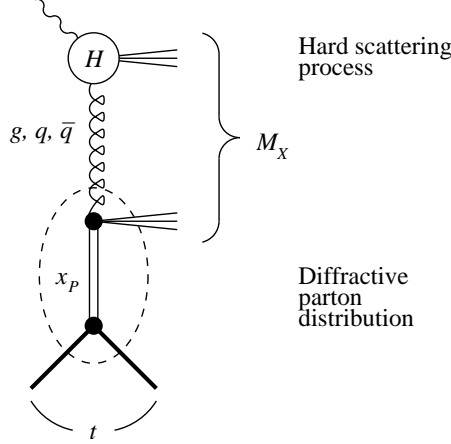


Figure 11: Factorization in diffractive DIS. The amplitude in the dashed blob, multiplied with its complex conjugate and summed over final states, defines the diffractive PDF. The internal structure of the dashed blob illustrates the assumption (25), which does not follow from the QCD factorization theorem.

is the fraction of the light-cone momentum of the target available for hard interactions in hadron h . Most of the current studies focus on diffractive kinematics, where $h = p$ and $1 - x_h = x_{\mathbb{P}} \leq 0.01$. The conditional parton distribution functions in this case are referred to as diffractive parton distribution functions (dPDF's), and denoted as f_j^D . In current data analysis it is usually assumed that the dependence of the dPDF's on $x_{\mathbb{P}}, t$ and β, Q^2 can be factorized as [81]

$$f_j^D(\beta, Q^2, x_{\mathbb{P}}, t) = f_{\mathbb{P}/p}(x_{\mathbb{P}}, t) f_j^D(\beta, Q^2), \quad f_{\mathbb{P}/p}(x_{\mathbb{P}}, t) = f(t) x_{\mathbb{P}}^{-2\alpha_{\mathbb{P}}(t)+2}. \quad (25)$$

This assumption is inspired by the soft Pomeron exchange model (which does not follow from the QCD factorization theorem) and referred to as Regge factorization, see Fig. 11. An additional term can be added to Eq. (25) in analogy to non-vacuum exchange in soft physics; it gives a small contribution below $x_{\mathbb{P}} \sim 0.01$ and dominates at $x_{\mathbb{P}} \geq 0.05$.

Extensive studies of hard diffractive channels have been performed at HERA. The inclusive diffractive cross section was measured both integrated over t (the so-called diffractive structure function, $F_2^{D(3)}$), and as a function of t for a limited range of $x_{\mathbb{P}}$. These measurements are mostly sensitive to the quark dPDF, while the gluon dPDF enters through scaling violations. Diffractive dijet production for real and virtual photons, as well as diffractive charm production, primarily probe the gluon dPDF. The analysis of these data on the basis of QCD evolution equations has led to the following conclusions:

- The data at $Q^2 \geq 4 \text{ GeV}^2$ are described by the universal dPDFs, consistent with the factorization theorem.
- $f_g(\beta, Q_0^2) \gg \sum_q f_q(\beta, Q_0^2)$ for the studied range of β . This conclusion was initially based on the weak scaling violation for $F_2^{D(3)}(\beta, Q^2)$ for large β , and was later confirmed by the studies of diffractive dijet production and charm production. However, the latter processes have so far been treated only in the LO approximation, and one should await the NLO analysis before drawing final conclusions.

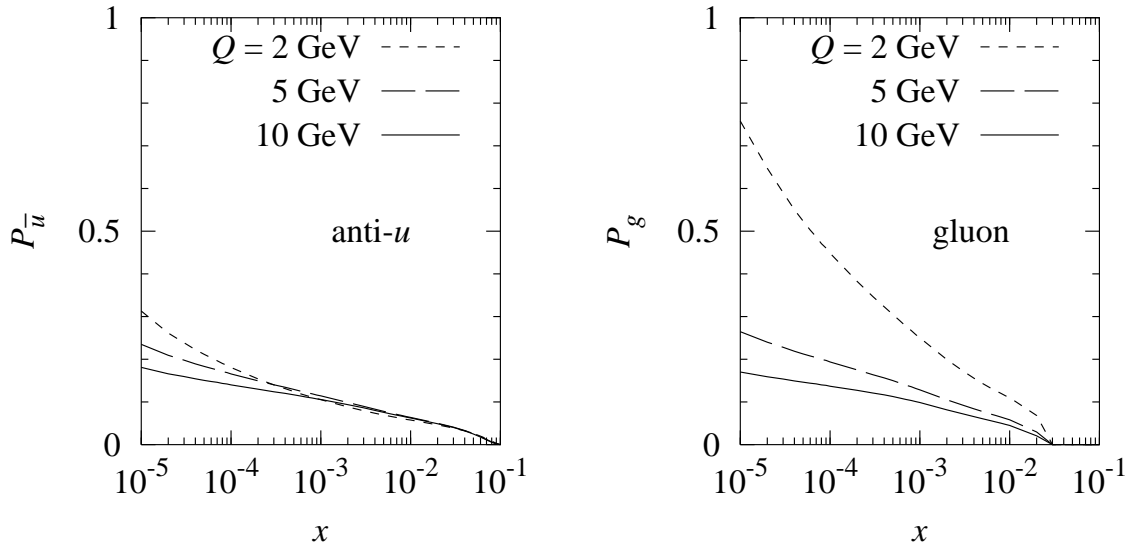


Figure 12: Probability of diffractive scattering from anti- u quarks (left) and gluons (right), extracted from a fit to the H1 data, see Ref. [82] (updated by V. Guzey).

- The data are consistent with Regge factorization, Eq. (25), although the $x_{\mathbb{P}}$ dependence is faster than in soft physics. The analysis of ZEUS and H1 diffractive data finds $\alpha_{\mathbb{P}}(t = 0) = 1.2 \pm 0.07$ and increasing with Q^2 , which should be compared with the energy dependence expected in soft hadronic collisions, $\alpha_{\mathbb{P}} \approx 1.1$.
- The absolute probability of diffraction in $\gamma^* + p$ scattering is of the order of 10% for moderate Q^2 , and thus of the same magnitude as in soft pion–nucleon collisions. However, the rate of increase of the diffractive cross section with energy for fixed M_X^2 and Q^2 is significantly faster than that of the total DIS cross section.

Another interesting characteristic of diffractive DIS is the probability of diffractive scattering depending on the type of parton coupling to the hard probe [72],

$$P_j(x, Q^2) = \int dt \int dx_{\mathbb{P}} f_j^D(x/x_{\mathbb{P}}, Q^2, x_{\mathbb{P}}, t) / f_j(x, Q^2). \quad (26)$$

This ratio cannot exceed the value 0.5, which corresponds to the unitarity (black disk) limit (BDL), *cf.* the discussion in Sec. 6. Using the H1 fit to the diffractive DIS data (see Fig. 12), we find $P_g \gg P_q$, and $P_g(x \sim 10^{-3}) \approx 0.4$ (0.3) for $Q^2 = 4$ (10) GeV^2 . That is, quark induced diffraction is small, whereas gluon induced diffraction is close to the maximum value allowed by unitarity. We shall return to this point in our discussion of the profile function for the dipole–nucleon interaction in Sec. 6. Note that the H1 fit is based on the data at $x \geq 10^{-4}$. The fact that it leads to $P_g \geq 0.5$ at smaller x indicates that the H1 parameterization should break down near the upper end of the HERA energy range.

5.2 Space–time picture of hard diffractive processes

To understand the observed pattern of hard diffraction, it is instructive to consider the space–time evolution of such processes in the target rest frame. Such studies reveal new information

about the interaction of small-size $q\bar{q}$ as well as $q\bar{q}g \dots g$ configurations with hadronic matter. In particular, the ratio of the diffractive to the total cross section probes the interactions of such configurations with the target without reference to the probe which created them.

An immediate consequence of the QCD factorization theorem is that, in the target rest frame, the number of components in the photon wave function evolves with Q^2 . While at low Q^2 an approximation by a few components in the photon wave function may be reasonable, it is definitely inappropriate for large Q^2 . This point is illustrated by the following example: Diffractive processes induced by longitudinally polarized photons are a leading-twist effect. If, however, all but the $q\bar{q}$ component of the photon wave function were neglected, one would erroneously conclude that diffraction is a higher-twist effect in this channel, because the transverse size of the longitudinal photon is $d^2 \propto 1/Q^2$. The proper Q^2 dependence is restored by the $q\bar{q}g \dots g$ configurations in the photon wave function.

At low Q^2 , aligned jet model-type configurations of large transverse size dominate in the wave function of the projectile photon, *cf.* Sec. 2.2. Such configurations interact with a hadronic cross section, $\sim \sigma_{\text{tot}}(\pi N)$, and thus have a significant probability to rescatter elastically. If Q^2 increases, these configurations cannot be effectively produced without emission of gluons. Because these gluons are predominantly emitted collinearly, they do not change the transverse size of the diffracting system, and hence the probability of elastic rescattering. Assuming smooth matching between the strength of interaction in the perturbative and nonperturbative regimes, models reasonably describe the data on hard diffraction in ep scattering if $P_g > P_q$ at the initial scale, Q_0^2 [83, 84]. Configurations of size $d^2 \geq \lambda/Q_0^2$, where $\lambda \approx 9$ (*cf.* the discussion in Sec. 3.2) should be included in the definition of the dPDF at the initial scale. For $Q_0^2 = 4 \text{ GeV}^2$, this includes rather small transverse sizes, for which the cross section increases with energy significantly faster than at the soft scale, which is consistent with the trend of the HERA data mentioned in Sec. 5.1. Also, because the $q\bar{q}g$ configurations have masses considerably larger than $q\bar{q}$ configurations, they should manifest themselves in diffraction at relatively small $\beta < 0.5$. Indications of diffraction into non-aligned jet final states were indeed found in a number of HERA experiments [85]. To summarize, it appears that hard diffraction at HERA with $Q^2 \sim 4 \text{ GeV}^2$ represents the border between the high- Q^2 region where leading-twist QCD dominates and the low- Q^2 region where higher-twist effects become important.

A quantitative analysis of the HERA data within the gluon dipole picture indicates that the interaction of gluon dipoles at HERA energies is rather close to the BDL [72], *cf.* the discussion in Sec. 6. However, due to our inability to build an effective trigger on the interaction of gluon dipoles with $d \geq 0.3 \text{ fm}$ it is difficult to observe this effect directly in the experiments.

To conclude this discussion, we briefly want to comment on the assumption of Regge factorization, Eq. (25). Because strong deviations of the energy dependence of diffraction from the soft regime are observed, there is a priori no reason for the validity of this assumption. Several effects are likely to contribute to the breakdown of Regge factorization: (a) different energy dependence of the cross section for diffraction of configurations of different transverse size, (b) emission of gluons by $q\bar{q}$ dipoles, which at smaller x occurs at large coherent lengths (*cf.* the discussion in Sec. 2.2), and (c) soft screening effects, which become more important with increasing energy (these effects were observed in soft diffraction [86, 87]), and which should be different for the various diffractive configurations, as they interact with different strengths.

One way to probe the degree of validity of Regge factorization is to check that the hadrons produced in the photon fragmentation region do not “talk” with hadrons in the target fragmentation region, *i.e.*, that there are no long-range correlations in rapidity. Such a factorization ignores the existence of color fluctuations, which lead to processes in which the proton also dissociates. If Regge factorization were valid, the probability of dissociation would not depend on the properties of the state into which the virtual photon has diffracted. However, if screening effects are present and non-universal (for example, due to the different strength of interaction in quark and gluon induced diffraction), Regge factorization should be broken.

5.3 Diffraction and leading-twist nuclear shadowing

A direct relation between diffraction in high-energy hadron-hadron collisions and the nuclear shadowing effect in hadron-nucleus collisions was derived by V. Gribov [88, 89], in the approximation where the nucleon radius is considerably smaller than the mean internucleon distance in nuclei. The same reasoning in conjunction with the leading-twist approximation for hard diffractive processes allows one to calculate nuclear shadowing of PDF's in light nuclei [72].

Application of the Abramovsky-Gribov-Kancheli cutting rules [90], which relate the shadowing phenomenon for the total cross section of high energy processes to that of partial cross sections (such as for diffraction, multiparticle production, *etc.*) and are valid in perturbative QCD (see Ref. [91] for a recent discussion), explicitly demonstrates that the interference of the amplitudes of diffraction from a proton and a neutron leads to a decrease of the total cross section for $\gamma^* D$ scattering. When combined with the factorization theorem for inclusive diffraction, one can calculate the modification of nuclear PDF's at low values of Bjorken x [72]. In the limit of low nuclear thickness, the nuclear shadowing corrections to the nuclear parton densities are given by

$$\begin{aligned} \frac{f_{j/A}(x, Q^2)}{A} &= f_{j/N}(x, Q^2) - \frac{1}{2} \int d^2b \int_{-\infty}^{\infty} dz_1 \int_{z_1}^{\infty} dz_2 \int_x^{x_0} dx_{\mathbb{P}} \cos[x_{\mathbb{P}} m_N (z_1 - z_2)] \\ &\times \frac{1 - \eta^2}{1 + \eta^2} f_{j/N}^D(\beta, Q^2, x_{\mathbb{P}}, t)_{|\mathbf{k}_{\perp}=0} \rho_A(b, z_1) \rho_A(b, z_2), \end{aligned} \quad (27)$$

where $f_{j/N}(x, Q^2)$ is the usual parton density in the proton, $f_{j/N}^D(\beta, Q^2, x_{\mathbb{P}}, t)$ the diffractive parton density (see Sec. 5.1), and $\rho_A(r)$ is the nucleon density in the nucleus with atomic number A . The momentum transfer, t , is given by $-t = (\mathbf{k}_{\perp}^2 + (x_{\mathbb{P}} m_N)^2)/(1 - x_{\mathbb{P}})$, where \mathbf{k}_{\perp} is the transverse component of the momentum, transferred to the struck nucleon, and $\beta = x/x_{\mathbb{P}}$. In Eq. (27), the factor $(1 - \eta^2)/(1 + \eta^2)$, where $\eta \equiv -\pi/2 \partial \ln(\sqrt{f_{i/N}^D})/\partial \ln(1/x_{\mathbb{P}}) = \pi/2 [\alpha_{\mathbb{P}}(t = 0) - 1]$, accounts for the real part of the amplitude of diffractive scattering [92]. One can easily modify Eq. (27) to include the dependence of the diffractive amplitude on t . Obviously, both the left- and right-hand side of Eq. (27) satisfy the QCD evolution equations in all orders in α_s , and this relation does not depend on the renormalization scheme. These expressions represent the model-independent result for leading-twist nuclear shadowing in the low-density limit.

In the case of heavy nuclei one may with good accuracy neglect the fluctuations of the strength of interaction in the hadron component of the photon wave function. This approximation makes it possible to extend the above formulas to the case of heavy nuclei [72, 93].

Numerical studies of shadowing using Eq. (27) and the corresponding expression for the total DIS cross section for heavy nuclei found large leading-twist shadowing effects for quark and gluon distributions, with gluon shadowing being larger up to rather high values of Q^2 . The latter effect can be traced to the higher probability of gluon-induced diffraction as compared to quarks, see Fig. 12.

The connection between diffraction and nuclear shadowing does not depend on the twist decomposition of the cross section, and was successfully applied also to data on nuclear shadowing of F_{2A} at intermediate Q^2 , see *e.g.* Refs. [94, 95]. One can use this to estimate the relative importance of leading-twist and higher-twist nuclear shadowing at $Q^2 \leq 2 \text{ GeV}^2$, using experimental information on the leading-twist contribution to the diffractive cross section at these values of Q^2 . One finds that a significant higher-twist contribution to diffractive DIS originates from ρ meson production. This implies that a significant fraction ($\sim 40\%$) of the nuclear shadowing observed in the experiments at CERN and Fermilab (see Ref.[76] for a review) may be due to higher-twist effects [93].

Recently, leading-twist nuclear shadowing was included in the initial conditions for the small- x evolution in the McLerran-Vegunopalan model [96]. A distinctive feature of this model is that the invariant masses in the nuclear vertex of the BFKL ladder should be very large as compared to Q^2 . That is, small β should dominate in the integral, in analogy to Eq. (27). A numerical analysis of gluon shadowing using the HERA dPDF's finds that the region $\beta \leq 0.1$ becomes important only for $x \leq 10^{-4}$. Thus, the assumption of the dominance of large diffractive masses may give rise to important dynamical effects at the next generation of accelerators.

5.4 Implications of nuclear shadowing for heavy-ion collisions

The typical x -values relevant for semihard production of hadrons in heavy-ion collisions decreases with energy as $x_A \sim 2p_\perp/\sqrt{s_{NN}}$ for central rapidities, and much faster, $\propto 1/s$, for the fragmentation regions (s_{NN} is the squared center-of-mass energy of the effective nucleon-nucleon collisions). For central rapidities and $p_\perp \geq 2 \text{ GeV}$, gluon shadowing is still a small correction at RHIC. However, it will be a large effect at LHC for a wide range of p_\perp , because the relevant x_A are much smaller than 0.01. The expected suppression of jet production is given by the factor $[G_A(x_A, p_\perp^2)/AG(x_A, p_\perp^2)]^2$, where G_A and G are the gluon densities in the nucleus and the nucleon, respectively. This factor can be of the order of 1/4 [82].

Because the current RHIC detectors have rather limited forward coverage, they have limited sensitivity to small- x phenomena. One exception is J/ψ production, which, if interpreted within perturbative QCD, probes x down to 0.003. The observed suppression of the J/ψ yield is consistent with the estimates of Ref.[93], see Ref. [97] for a review. The A -dependence of forward high- p_\perp hadron production was studied by BRAHMS [98]. Although at large rapidities small x contribute to the high p_\perp spectra, the QCD analysis indicates that average x are ~ 0.03 [99]. Consequently, the yields are practically not sensitive to the shadowing effects, or, more generally, to any initial-state modifications of the nucleus wave function. Final-state interaction effects which could explain the data are nonperturbative contributions to the production of leading hadrons, due to coalescence of spectator partons and the relatively small energy losses in the initial and final state (on the scale of 3%).

6 Black–disk limit in dipole–hadron interactions

6.1 Violation of the leading–twist approximation at small x

A fundamentally new dynamical effect expected at high energies is the unitarity limit, or black–disk limit (BDL), in the interaction of a small dipole with hadronic matter. We now describe and quantify this effect, using the information gathered in our studies of inclusive, exclusive and diffractive DIS in Sections 3, 4 and 5.

A simple argument shows that the twist expansion for the cross sections of hard processes breaks down at sufficiently small x . QCD factorization predicts that the total cross section for DIS at fixed Q^2 increases with decreasing x as $\sigma_{\text{tot}} \propto xG(x)/Q^2$. At the same time, the cross section of elastic dipole–hadron scattering (which corresponds to the production of diffractive states with masses $M_X \propto 1/d \propto Q$) grows much faster, $\sigma_{\text{diff}} \propto (xG)^2/(BQ^4)$, where B is the t –slope of the corresponding differential cross section [21]. Clearly, at sufficiently small x there is a contradiction — the total cross section should always be larger than that for any particular channel [44]. The resolution of this paradox is that the decomposition of hard amplitudes in powers of $1/Q^2$ becomes inapplicable at sufficiently small x .

In order to quantify the onset of the new regime, it is instructive to consider the effects of unitarity (conservation of probability) on a purely theoretical scattering process, namely the scattering of a $q\bar{q}$ (quark–antiquark) or gg (gluon–gluon) dipole of small transverse size, d , from a hadronic target. Neglecting other constituents in the dipole is justified in a wide kinematic range by the smallness of the coupling constant; large terms $\propto \alpha_s \ln(x_0/x)$ arise only from interactions at large rapidity intervals. The invariant amplitude for dipole–proton elastic scattering is a function of the invariants $s \equiv W^2$, and t . We write it as a Fourier integral over the dipole–proton impact parameter, b ,

$$A^{dp}(s, t) = \frac{is}{4\pi} \int d^2b e^{-i(\Delta_\perp b)} \Gamma^{dp}(s, b) \quad (t = -\Delta_\perp^2), \quad (28)$$

where $\Gamma^{dp}(s, b)$ is the so–called profile function. Making use of unitarity, one can express the total, elastic, and inelastic (total minus elastic) cross sections in terms of the profile function as

$$\left. \begin{array}{l} \sigma_{\text{tot}}(s) \\ \sigma_{\text{el}}(s) \\ \sigma_{\text{inel}}(s) \end{array} \right\} = \int d^2b \times \left\{ \begin{array}{l} 2 \text{Re} \Gamma^{dp}(s, b) \\ |\Gamma^{dp}(s, b)|^2 \\ [1 - |1 - \Gamma^{dp}(s, b)|^2] \end{array} \right\}. \quad (29)$$

In the situation where elastic scattering is the “shadow” of inelastic scattering, the profile function at a given b is restricted to values $|\Gamma^{dp}(s, b)| \leq 1$. The value $\Gamma^{dp}(s, b) = 1$ corresponds to complete absorption at a given impact parameter, the so-called black disk limit (BDL).⁴

The proximity of $\Gamma^{dp}(s, b)$ to unity is an important measure of the strength of the interaction of the dipole with the proton. As outlined in Sec. 2.2, the analysis of γ^*N scattering in the target

⁴In non-relativistic quantum mechanics, the scattering of a particle from a completely absorptive sphere is referred to as the “black–body limit.” In contrast, the high–energy limit of scattering amplitudes in QCD is essentially two–dimensional, with the radius of interaction increasing with energy. It is thus natural to refer to the limit of complete absorption as the “black disk limit.”

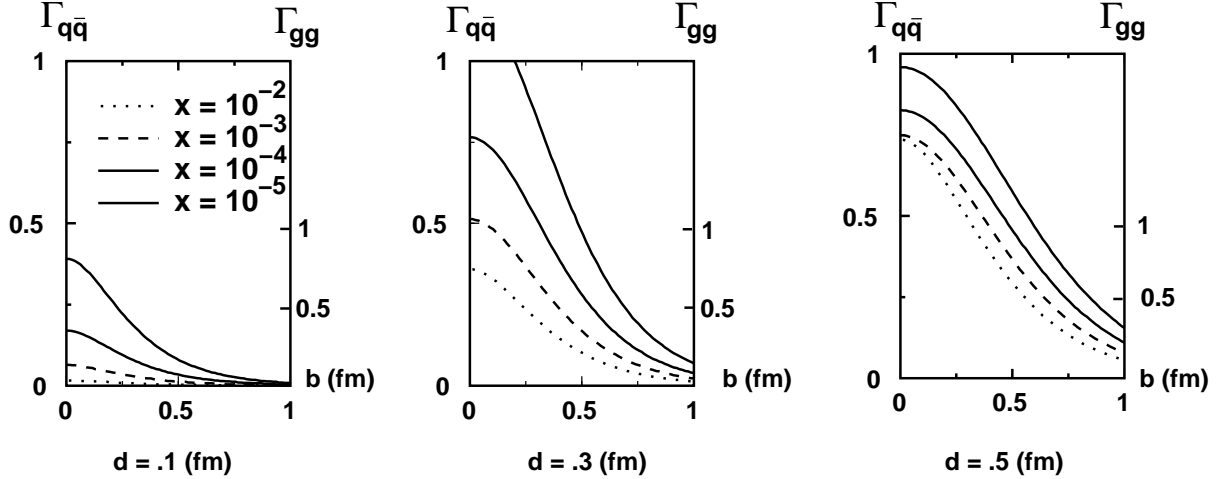


Figure 13: The profile function of dipole–nucleon scattering, Γ^{dp} , as a function of the impact parameter, b , for various values of the dipole size, d , and x , as obtained from a phenomenological estimate (see text).

rest frame allows one to determine with reasonable accuracy (LO approximation) the total cross section for the scattering of a $q\bar{q}$ dipole from the proton. Combining this with information on the transverse spatial distribution of gluons in the nucleon, obtained from measurements of the t –dependence of exclusive J/ψ photoproduction and other hard exclusive processes (*cf.* Sec. 4.4), we can calculate the profile function for dipole–nucleon scattering [73]. A sample of the results of Ref. [100] is presented in Fig. 13. Here, $x = Q^2/s$, where $Q^2 = \lambda/d^2 \approx 9/d^2$ is the characteristic virtuality corresponding to the dipole size. One sees that up to the top of the HERA energy range, $x \sim 10^{-4}$, the profile function for a $q\bar{q}$ dipole remains small for dipole sizes $d \leq 0.3$ fm, corresponding to $Q^2 \geq 4$ GeV², the value usually used as a starting point for DGLAP evolution [101]. Even for larger dipole sizes, $d \sim 0.5$ fm, the fraction of the cross section due to scattering with $\text{Re } \Gamma \geq 0.5$ remains small. This shows that the BDL is not reached in inclusive DIS at HERA energies, in agreement with what we observed in Sec. 3.1 and 3.2. However, the DGLAP evolution starting from a $q\bar{q}$ dipole generates gg dipoles, whose interaction at leading twist is larger by a factor of 9/4, *cf.* Eq. (8), and thus approaches the BDL much earlier. The theoretical estimate shown in Fig. 13 indicated that the strength of interaction of gg dipoles is close to maximal at the top of the HERA energy range, for a wide range of b , and dipole sizes corresponding to $Q^2 \leq 4$ GeV². This implies that in gluon–induced interactions at HERA at such Q^2 the probability of diffraction should be close to 1/2 — exactly as we found in the analysis of HERA diffractive data in Sec. 5.1.

To summarize, one may expect that the leading–twist approximation for DIS breaks down for $Q^2 \leq 4$ GeV², especially in the gluon sector. Unfortunately, there are no readily available probes of gluons at low Q^2 , except possibly the longitudinal cross section, σ_L . Without such measurements, it is impossible to determine whether the successful DGLAP fits to the HERA data down to $Q^2 \sim 1$ GeV² are an artifact of using an essentially arbitrary gluon density at low Q^2 and low x ; this function is practically not constrained by the data at larger Q^2 , where it is dominated by DGLAP evolution from larger x . Also, it is worth emphasizing that although $\Gamma^{dp}(b)$ for gluon dipoles (and, at higher energies, also for quark dipoles) reaches values close to

unity, the actual deviation of the nucleon structure function from the DGLAP fits may still be rather small, as the contributions from scattering at large b remain dominant.

6.2 Theoretical issues in describing the black-disk limit

The analysis of the full DGLAP evolution equation and the resummation approaches shows that the cross section for the scattering of a small dipole increases effectively as x^{-n} , with $n \geq 0.2$ for $Q^2 \sim \text{few GeV}^2$, and somewhat faster at larger Q^2 . [At very large Q^2 and extremely high energies — well above the LHC range — the resummation approaches predict that $n \propto \alpha_s(Q^2)$, and thus $n \rightarrow 0$.] Within these approximations, the t -slope of the differential cross section for elastic dipole-nucleon scattering, B , increases with energy rather slowly, *cf.* the discussion in Sec. 4.4. Thus, the cross section for dipole-nucleon elastic scattering increases with energy faster than the total cross section, and unitarity is violated for this hard processes within the leading-twist approximation (see the discussion in Sec. 6.1). Probability conservation will be violated at fixed impact parameter, b , in a region corresponding to a disk of finite size. At large enough b , the interaction is too small to violate the leading-twist approximation. Note that in soft interactions the increase of the elastic cross section does not necessarily lead to a contradiction with unitarity, because soft interactions generate also α' , and therefore give rise to an increase of the t -slope as $B \propto \ln s$.

The conventional assumption is that, beyond the leading-twist approximation, taming of the growth of cross sections occurs due to the shadowing phenomenon (this follows *e.g.* from V. Gribov's reggeon calculus). Specific to this phenomenon is that bare particles may experience only one inelastic collision, but any number of elastic interactions, without changing trajectory. The behavior of the amplitudes for high-energy processes in QCD differs from that given by the eikonal approximation in non-relativistic quantum mechanics because of the necessity to account for the non-conservation of the number of bare particles. Application of the Abramovsky-Gribov-Kancheli cutting rules [90] shows that the requirement of positive probabilities for total cross sections, single particle densities, *etc.*, impose serious restrictions on the dynamics in the case of cross sections increasing with energy. To satisfy these requirements in a series of multiple rescatterings in which consecutive terms have alternating signs, the effective number of constituents in the dipole wave function should increase with energy. Thus, the increase of the cross section with energy leads to resolution of constituents in the wave functions of the colliding particles, and therefore to an evolution of final states. Evolution and gluon emission by dipoles are the key for generating multiple inelastic collisions without violation of causality and energy-momentum conservation. The evolution of a dipole in time manifests itself in the expansion of the system, emission of gluons, transitions between components containing different numbers of bare particles, change of impact parameters in the intermediate states, and the related effect of the cross section for inelastic diffraction exceeding the elastic cross section for the scattering of small dipoles, *cf.* the discussion in Sec. 5. In this regime, the concept of a parton density of the target cannot be defined in a model-independent way, because the parton distributions in the dipole and the target are intertwined and not restricted by probability conservation.

At energies where the dipole cross section becomes comparable or even larger than $2\pi R_N^2$, the whole picture of rescattering becomes inconsistent if the radius squared of the interaction

is not proportional to the dipole cross section. For example, in this case the Glauber approximation for hadron–deuteron scattering would lead to negative total cross sections. Fortunately, in QCD the wave function of a fast projectile contains many partons. This fact, combined with the increase of the dipole cross sections with energy, is sufficient to ensure complete absorption for central collisions, without detailed knowledge of the hadron wave function [102]. To illustrate the rapid onset of complete absorption for central collisions related to the increase of the number of constituents, we adopt here a simple approximation, namely that the perturbative QCD (pQCD) description of dipole–proton scattering works up to $\text{Re } \Gamma^{dp}(b, x) = 1$, and that $\Gamma^{dp}(b, x) = 1$ if the pQCD formulas lead to $\text{Re } \Gamma^{dp}(b, x) > 1$. That is,

$$\begin{aligned} \text{Re } \Gamma^{dp}(b, x) &= \text{Re } \Gamma^{dp}(b, x)_{\text{pQCD}} \Theta [1 - \text{Re } \Gamma^{dp}(b, x)_{\text{pQCD}}] \\ &+ \Theta [\text{Re } \Gamma^{dp}(b, x)_{\text{pQCD}} - 1]. \end{aligned} \quad (30)$$

Many of the models currently discussed in the literature use the elastic eikonal approximation to describe the taming of the increase of the dipole–hadron cross section with energy as due to the shadowing phenomenon, see *e.g.* Refs. [103, 104] for a nucleon target and Refs. [105] for a heavy nuclear target. These models assume that taming becomes significant for $\Gamma^{dp}(b) \geq 0.5$, *i.e.* at significantly larger x than the values where unitarity is explicitly violated in the pQCD approximation. Early taming results in a slow approach to the unitarity limit, $\Gamma^{dp}(b) = 1$. Obviously, these conclusions are model dependent, as such models neglect most of the QCD effects mentioned above.

The condition of the BDL for dipole–hadron scattering, $\Gamma^{dp}(b) = 1$, expresses the complete “loss of memory” of the cross section on the structure of the projectile and the target, and of the value of the running coupling constant, in a finite region of transverse space. It reflects the breakdown of two–dimensional conformal invariance (which is the basis of approximate Bjorken scaling in DIS) because of the appearance of a dynamical scale related to the high gluon density and the radius of the transverse distribution of gluons. The qualitative departure from pQCD dynamics in the BDL cannot be explained as a soft interaction effect. This can be understood when considering collisions of two small dipoles of same size near the BDL, *e.g.* $\gamma^*(Q^2)$ – $\gamma^*(Q^2)$ scattering at sufficiently large Q^2 , in which soft interaction effects are under control and negligible. An interesting question is whether, from a general perspective, the appearance of this new scale corresponds to a spontaneous breakdown of conformal symmetry, or is related to the conformal anomaly.

6.3 High–energy limit of nuclear and hadronic structure functions

The approach to the BDL in dipole–hadron scattering at high energies has interesting implications for the theoretical behavior of hadron and nuclear structure functions at extremely high energies, which is subject to the Froissart bound.

We consider the scattering of a virtual photon from a heavy nucleus (radius R_A) at high energies as a superposition of the scattering of dipoles of different sizes. The interaction at impact parameters $b \leq R_A$ will be black for dipoles with sizes larger than some critical size, $d > d(x)$, leading to a contribution to the cross section [*cf.* Eq. (11)]

$$\sigma^{\gamma^*A} \approx 2\pi R_A^2 \int d^2d \int_0^1 dz |\psi^\gamma(d, z)|^2 \Theta[d - d(x)]. \quad (31)$$

Because the profile function of dipole–nucleus scattering increases like a power of energy in the region where it is < 1 , one concludes that $d(x) \propto x^m$, with $m > 0$. When the nuclear radius significantly exceeds the essential impact parameters in γ^*N collisions, one has

$$F_{2A}(x, Q^2) = \frac{Q^2}{12\pi^3} \left(\sum_f e_f^2 \right) (2\pi R_A^2) \ln \frac{x_0(Q^2)}{x}, \quad (32)$$

where $x_0(Q^2)$ slowly decreases with increasing Q^2 .⁵ For illustrative purposes, we neglect here the contributions from peripheral collisions, which grow with the atomic number as $A^{1/3}$. Although formally these contributions increase with energy faster than those from central collisions (which are nearly energy–independent), they are still comparatively small at all achievable energies. The gross violation of Bjorken scaling in Eq. (32), $F_{2A} \propto Q^2 \ln(x_0/x)$, and the numerical coefficient follow from the normalization of the photon wave function to the Q^2 –derivative of the photon polarization operator, as opposed to unity as for hadron wave functions. Equation (32) represents a QCD modification of the Gribov BDL [89], which assumed that all configurations in the virtual photon with masses $M^2 \leq 2m_N x/R_A$ interact with the heavy nucleus with maximum strength.

In DIS from a proton target scattering at large impact parameters is always important in the regime where the pQCD interaction becomes strong. Indeed, based on the studies of the transverse spatial distribution of gluons in hard exclusive processes (see Sec. 4.4) one expects that $\Gamma^{dp}(s, b) \propto \exp(-\mu b)$ at large b , with $\mu \approx m_g$ for moderately small x [cf. Eq. (22)], and $\mu \rightarrow 2m_\pi$ in the limit of infinitely large energies. It follows from the unitarity bound, Eq. (29), that the essential impact parameters increase with energy as $b^2 \propto \mu^{-2} \ln^2[\sigma(s, d)/(8\pi B)]$, where B is the t –slope of the differential cross section of dipole–nucleon scattering, which is almost energy–independent within the leading–twist approximation. The cross section of dipole–nucleon scattering therefore increases with energy as [106]

$$\sigma \propto \mu^{-2} \ln^2 \frac{\sigma(s, d)}{8\pi B}. \quad (33)$$

In general, this behavior differs from the Froissart limit for soft hadronic interactions, because of the more complicated dependence of the dipole cross section, $\sigma(s, d)$, on the energy, as described by the resummation approaches. To simplify the formulas, below we shall use the observation that effectively $\sigma(s, d) \propto s^{n(d)}$, with $n \geq 0.2$ for small d . This approximation leads to the limiting behavior familiar from soft hadronic interactions [3]. The leading asymptotic term in x for fixed Q^2 for the nucleon structure function is

$$F_2(x, Q^2) = \frac{Q^2}{12\pi^3} \left(\sum_f e_f^2 \right) \sigma \ln \frac{s}{s_0} \propto \ln^3 \frac{s}{s_0}, \quad (34)$$

where two logarithms originate from the dipole–nucleon cross section, and one from the integral over the photon wave function, similar to the case of scattering from nuclei.

⁵Since in the BLD the masses of the intermediate states are much larger than Q^2 , the coherence length is much smaller than the naive estimate, $l_{\text{coh}} \sim 1/(2m_N x)$. If the gluon density in the approach to the BDL grows as $x^{-\lambda(Q^2)}$, one expects that $l_{\text{coh}} \propto 1/(m_N x^{1-\lambda})$.

In hard exclusive processes in γ^*p scattering, the approach to the BDL implies that the t -slope increases with energy $\propto \ln^2(s/s_0)$ (*cf.* also Sec. 7.4). A promising strategy in searching for BDL effects would be to extract partial waves for small impact parameters from the cross sections of processes such as DVCS from the nucleon, ρ -meson production [107], coherent photoproduction of high p_\perp dijets from the nucleon, and coherent photoproduction of $J/\psi, \psi', \psi''$ mesons. This would allow one to probe small b , where the gluon density is maximal and unitarity effects should manifest themselves early. Another possible strategy is to study the structure functions of heavy nuclei, where due to higher gluon densities the BDL effects are enhanced by a factor $A^{1/3}$ [108]. Note that this enhancement is partly compensated by nuclear shadowing; *cf.* the discussion in Sec. 5.3.

It is interesting also to explore the behavior of nuclear structure functions at extremely high energies, where the radius of the γ^*N interaction becomes comparable to or even exceeds the nuclear radius. In this case, first the edge of the nucleus contributes terms $\propto A^{1/3} \ln(x_0/x)^3$ to the cross section. Ultimately, for $s \rightarrow \infty$ and fixed Q^2 , one would reach the universality regime where $F_{2A}(x, Q^2)/F_{2p}(x, Q^2) \rightarrow 1$ [102]. However, the relevant scale is comparable to the gravitational scale.

6.4 Black-disk limit in hard diffractive scattering from heavy nuclei

An important consequence of the BDL is that, in diffractive scattering at high energies, non-diagonal transitions between diffractive eigenstates are forbidden [89]. This follows from the orthogonality of the eigenstates — if every configuration in the projectile interacts with the same strength, the relative proportion between different configurations remains the same. This implies that half of the nuclear DIS cross section should be due to diffraction, with the nucleus remaining intact, and a “jetty” diffractive final state resembling that of $e^+e^- \rightarrow$ hadrons. In contrast, in the leading-twist approximation this cross section should be negligible.

At the onset of the BDL regime, where the contributions from configurations in the virtual photon interacting with the BDL strength and those for which pQCD is applicable are comparable, one can calculate the differential cross section for diffraction to final states of small mass, M_X , for which the interaction is already black,

$$\frac{dF_T^{\gamma^* \rightarrow X}(x, Q^2, M_X^2)}{dM_X^2 d\Omega_X} = \frac{\pi R_A^2}{12\pi^3} \frac{Q^2 M_X^2}{(M_X^2 + Q^2)^2} \frac{d\sigma(e^+e^- \rightarrow X)/d\Omega_X}{\sigma(e^+e^- \rightarrow \mu^+\mu^-)}. \quad (35)$$

This shows a much slower decrease with Q^2 than in the leading-twist approximation, and corresponds to “jetty” final states (mostly diffraction to $q\bar{q}$ and $q\bar{q}g$ jet states). The earliest signal for the change of Q^2 dependence should be in ρ meson production, where the Q^2 dependence of the dominant longitudinal cross section should change from $1/Q^6$ (see Sec. 4.3) to $1/Q^2$.

Theoretical studies show that at HERA kinematics the fraction of the cross section due to diffraction should be much closer to 1/2 for nuclear targets than for the proton [109]. The use of nuclear beams would greatly facilitate the exploration of the BDL regime. Possibilities for such measurements in ultraperipheral collisions at LHC will be discussed in Sec. 9.

7 Small- x dynamics in hadron–hadron collisions

7.1 Transverse radius of hard and soft interactions

Our studies of γ^*p scattering at HERA have taught us several important lessons about the gluon density at small x , the transverse spatial distribution of gluons, and about the interaction of small-size color singlets with hadrons (see Sec. 1 for a summary). We now explore the implications for the physics of $pp/p\bar{p}$ and pA collisions at high energies.

In hadron–hadron collisions, hard processes arise from binary collisions of partons in the colliding hadrons, in which a system of large invariant mass, $M^2 \gg \Lambda_{\text{QCD}}^2$, is produced. Examples are the production of dijets, dilepton pairs (Drell–Yan process), and the production of heavy particles such as Higgs bosons or SUSY particles. Such hard partonic processes are generally accompanied by a rich spectrum of soft interactions, which dominate the total hadronic cross section and determine the overall characteristics of hadron production in the final state. Understanding the interplay of hard and soft interactions is the main challenge in describing hadron–hadron collisions with hard processes.

A crucial observation in studies of hard exclusive processes in γ^*p scattering is that gluons with significant momentum fraction ($x > 10^{-3}$) are concentrated in a transverse area much smaller than that associated with the nucleon in pp elastic scattering at high energies, which is dominated by soft interactions. The difference between the two areas becomes more pronounced with increasing energy. When considering the production of a system of fixed mass, M^2 , in collision of partons with $x_1 x_2 = M^2/s$, the transverse area of the hard partons grows with energy as $\langle \rho^2 \rangle = \alpha'_{\text{hard}} \ln s$, whereas the transverse area for soft interactions grows at a much faster rate, $\alpha'_{\text{soft}} \gg \alpha'_{\text{hard}}$. The cause of this difference is the suppression of Gribov diffusion for partons of large virtuality, as described in Sec. 2.2. Thus, in high-energy pp collisions one is dealing with an “onion-like” transverse structure of the nucleon (two-scale picture), see Fig. 14a.

The two-scale picture of the transverse structure of the nucleon implies a classification of $pp/p\bar{p}$ events in “central” and “generic” collisions, depending on whether the transverse areas occupied by the large- x partons in the two protons overlap or not, see Fig. 14b [73]. Generic collisions give the dominant contribution to the overall inelastic cross section. Hard processes, such as heavy particle production at central rapidities, will practically happen in central collisions only. (Obviously, in these collisions multiparton interactions due to the small- x gluon fields are strongly enhanced, giving rise to the dynamical effects described in the following subsections.)

To quantify the distinction between generic and central collisions, we estimate the distribution of the probability for both types of events over the impact parameter of the pp collision, b . For generic collisions, the distribution is determined by the b -dependent probability of inelastic interaction, obtained via unitarity from the elastic pp amplitude in the impact parameter representation, Eq. (29). We define a normalized b -distribution as

$$P_{\text{in}}(s, b) = [2\text{Re } \Gamma^{pp}(s, b) - |\Gamma^{pp}(s, b)|^2] / \sigma_{\text{in}}(s), \quad (36)$$

where $\sigma_{\text{in}}(s)$ is the inelastic cross section, which is given by the integral $\int d^2b$ of the expression in the numerator. For collisions with a hard process, on the other hand, the b -distribution

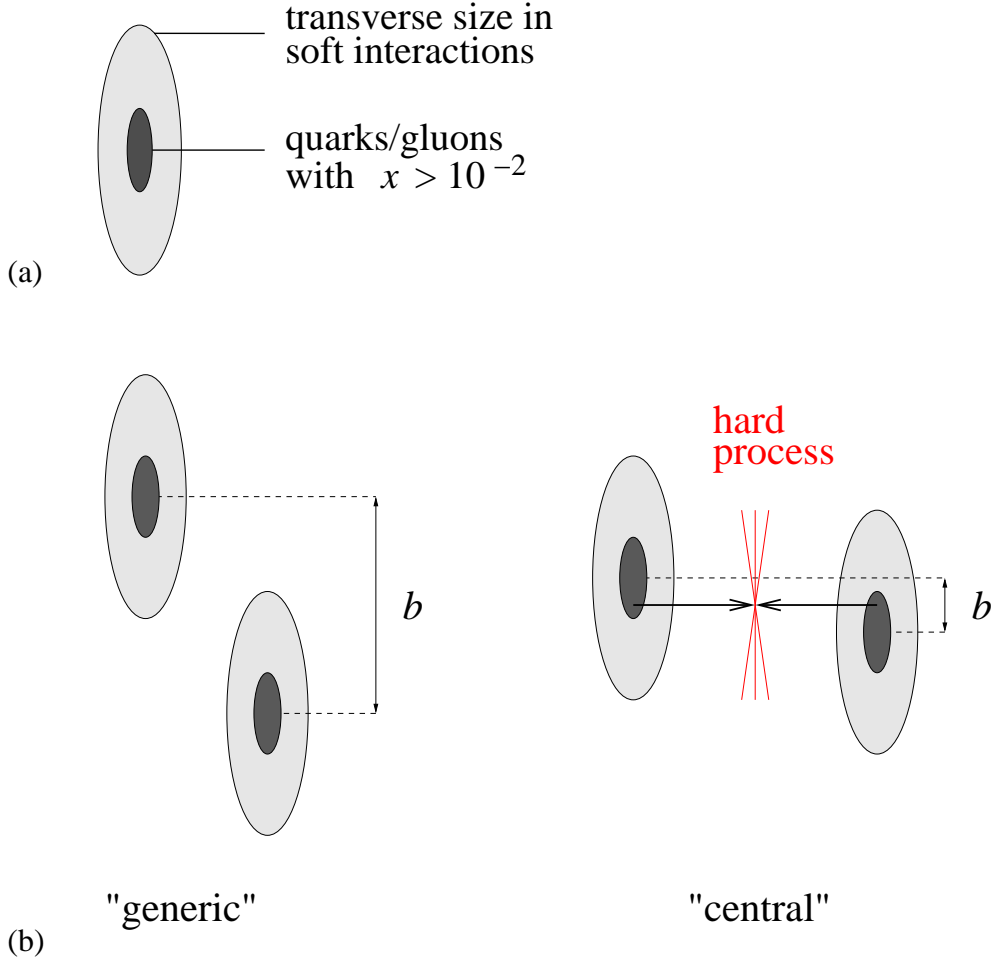


Figure 14: (a) The two-scale picture of the transverse structure of the nucleon in high-energy collisions. (b) The resulting classification of $pp/\bar{p}p$ events in “generic” and “central” collisions.

is determined by the overlap integral of the distribution of hard partons in the two colliding protons (see Fig. 14b),

$$P_2(b) \equiv \int d^2\rho_1 \int d^2\rho_2 \delta^{(2)}(\mathbf{b} - \boldsymbol{\rho}_1 + \boldsymbol{\rho}_2) F_g(x_1, \rho_1) F_g(x_2, \rho_2). \quad (37)$$

Numerical estimates can be performed with our parametrization of the transverse spatial distribution of hard gluons, see Sec. 4.4, which takes into account the change of the distribution with x and the scale of the hard process. The two b -distributions are compared in Fig. 15 for Tevatron and LHC energies. For the hard process we have taken the production of a dijet with transverse momentum $q_\perp = 25$ GeV at rapidity $y = 0$ in the center-of-mass frame; in the case of Higgs production at LHC the distribution $P_2(b)$ would be even narrower. The results clearly show that events with hard processes have a much narrower impact parameter distribution than generic inelastic events.

One expects that at LHC energies the rate of production of two pairs of jets will be very high. It is interesting to consider the b -distribution also for the production of two dijets in two

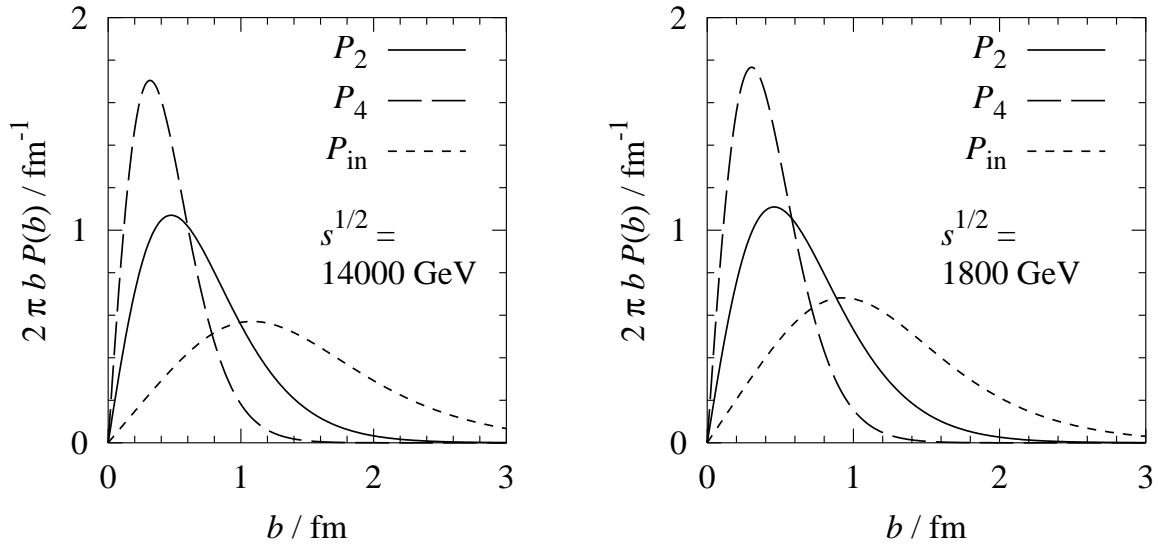


Figure 15: *Solid lines*: Impact parameter distributions in events with hard dijet production, $P_2(b)$, in pp collisions at LHC (left panel) and $\bar{p}p$ collisions at the Tevatron (right panel), for a back-to-back dijet at zero rapidity with transverse momentum $q_\perp = 25$ GeV. *Long-dashed lines*: Same for double dijet events, $P_4(b)$. *Short-dashed lines*: Impact parameter distributions in generic inelastic collisions, obtained from the parameterization of the elastic pp amplitude of Islam *et al.* [110]. The plots show the “radial” distributions in the impact parameter plane, $2\pi b P(b)$.

binary parton-parton collisions. Neglecting possible correlations between the partons in the transverse plane it is given by

$$P_4(b) \equiv [P_2(b)]^2 / \int d^2b [P_2(b)]^2. \quad (38)$$

Fig. 15 shows that this distribution is significantly narrower than P_2 , *i.e.*, the requirement of two hard processes results in a further reduction of effective impact parameters.

Correlations in the transverse positions of partons can be probed by studying $pp/\bar{p}p$ events with two hard processes, involving two binary collisions of partons. At the Tevatron such a process — production of three jets and a photon — was studied by the CDF collaboration [111]. The observed cross section is by a factor of 4 larger than the naive estimate based on the assumption that the partons are distributed uniformly in the transverse plane, over an area whose size was inferred from the proton electromagnetic form factor. The effect of correlations in the transverse position of partons (*i.e.*, their localization in “spots” of significantly smaller size than the radius of their distribution within the nucleon) reduces this discrepancy by a factor of 2. This hints at the presence of significant correlations in the parton transverse positions for $x \geq 0.05$. A possible explanation of such correlations is the localization of the non-perturbative gluon fields in “constituent” quarks (and antiquarks), as suggested by the instanton vacuum model of chiral symmetry breaking in QCD and supported by a large body of information on low-energy hadron structure, see Ref. [31] for a review. We find that the parton correlations implied by this model indeed give rise to a further enhancement of the cross section for two hard processes by a factor ~ 2 , see Refs. [73, 112] for details.

7.2 Black–disk limit in high–energy pA and pp collisions

A new effect encountered in high–energy pA and pp collisions is that the interaction of leading partons in the proton with the gluon field in the nucleus (or other proton) approaches the maximum strength allowed by s –channel unitarity, the BDL. This leads to certain qualitative modifications of the hadronic final state, which will be observable in central pp and pA collisions at LHC. In particular, this effect dramatically changes the strong interaction environment for new heavy particle production in central pp collisions at LHC.

In a high–energy pA collision, consider a leading parton in the proton, with longitudinal momentum fraction $x_1 \sim 10^{-1}$ and typical transverse momentum of the order of the inverse hadron size; see Fig. 16. Assuming a leading–twist two–body scattering process with transverse momentum p_\perp in the final state, this leading parton can interact with partons in the nucleus of momentum fraction

$$x_2 = \frac{4p_\perp^2}{x_1 s} \quad (39)$$

(x_2 and s here refer to the effective pN collision). If s becomes sufficiently large, x_2 can reach very small values even for sizable transverse momenta, $p_\perp^2 \gg \Lambda_{\text{QCD}}^2$. For example, at LHC $x_2 \sim 10^{-6}$ is reached for $p_\perp \approx 2 \text{ GeV}$. At such values of x_2 , the gluon density in the nucleus becomes large. The leading parton can be thought of as propagating through a dense “medium” of gluons. In this situation, the probability for the leading parton to split into several partons and scatter inelastically approaches unity, corresponding to the scattering from a “black” object. As a result the leading parton effectively (via splittings) undergoes inelastic collisions, losing energy and acquiring transverse momentum, until its transverse momentum is so large that the interaction probability becomes small, and the nucleus no longer appears “black”. To summarize, we can say that in pA collisions the leading partons acquire transverse momenta of the order of the maximum transverse momentum for which their interaction with the nucleus

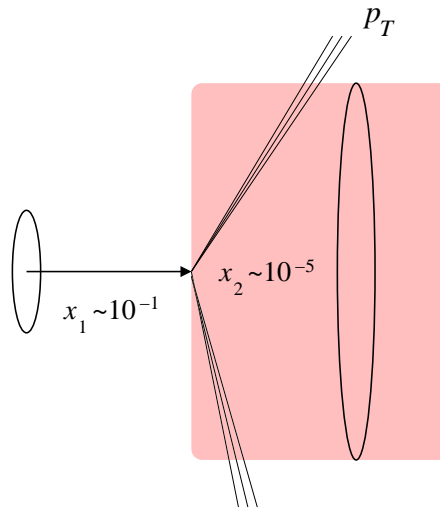


Figure 16: The black–disk limit (BDL) in central pA collisions: Leading partons in the proton, $x_1 \sim 10^{-1}$, interact with a dense medium of small– x_2 gluons in the nucleus (shaded area), acquiring a large transverse momentum, p_\perp .

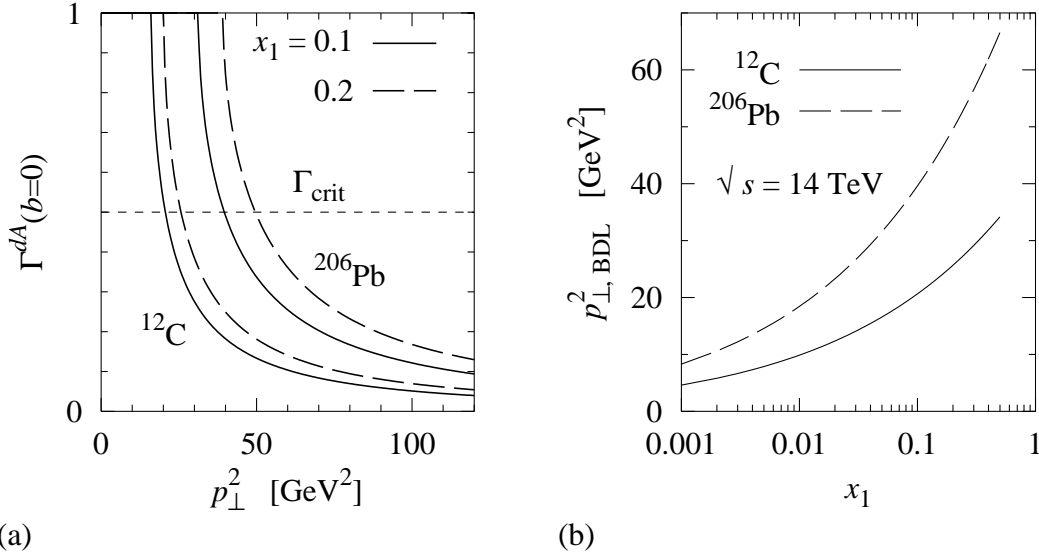


Figure 17: Black-disk limit in central pA collisions at LHC: (a) The profile function for the scattering of a leading gluon in the proton (regarded as a constituent of a gg dipole) from the nucleus at zero impact parameter, $\Gamma^{dA}(b = 0)$, as a function of the transverse momentum squared, p_{\perp}^2 . (b) The maximum transverse momentum squared, $p_{\perp,\text{BDL}}^2$, for which the interaction of the leading gluon is “black”, $\Gamma^{dA} > \Gamma_{\text{crit}}$, as a function of the gluon’s momentum fraction, x_1 . Here we assume $\sqrt{s} = 14$ TeV for the effective NN collisions, in order to facilitate comparison with the case of central pp collisions in Fig. 18.

at their respective x_1 is close to the BDL, $p_{\perp,\text{BDL}}$. This transverse momentum represents a new hard scale in high-energy hadron-hadron collisions, which appears because of the combined effect of the rise of the gluon density at small x and the unitarity condition.⁶

To estimate the maximum transverse momentum for interactions close to the BDL, we can treat the leading parton as one of the constituents of a small dipole scattering from the target. This “trick” allows us to apply the results of Sec. 6 to hadron-hadron scattering. In this analogy, the effective scale in the gluon distribution is $Q_{\text{eff}}^2 = 4p_{\perp}^2$, corresponding to an effective dipole size of $d \approx 3/(2p_{\perp})$. For simplicity, we first consider the case of central collisions of a proton with a large nucleus, which allows us to neglect the spatial variation of the gluon density in the target in the transverse direction. This amounts to approximating the transverse spatial distribution of gluons in the nucleus by

$$G_A(x, \rho; Q_{\text{eff}}^2) \approx \frac{G_A(x; Q_{\text{eff}}^2)}{\pi R_A^2} \quad (\rho < R_A). \quad (40)$$

As a criterion for the proximity to the BDL, we require that the profile function of the dipole-nucleus amplitude at zero impact parameter satisfy $\Gamma^{dA}(b = 0) > \Gamma_{\text{crit}}$, see Fig. 17a. For an estimate, we choose $\Gamma_{\text{crit}} = 0.5$, corresponding to a probability for inelastic interaction of

⁶The kinematics of the final state produced in the interaction of the large- x_1 parton with the small- x_2 gluon field resembles the backscattering of a laser beam off a high-energy electron beam. The large- x_1 parton gets a significant transverse momentum and loses a certain fraction of its longitudinal momentum, accelerating at the same time a small- x_2 parton.

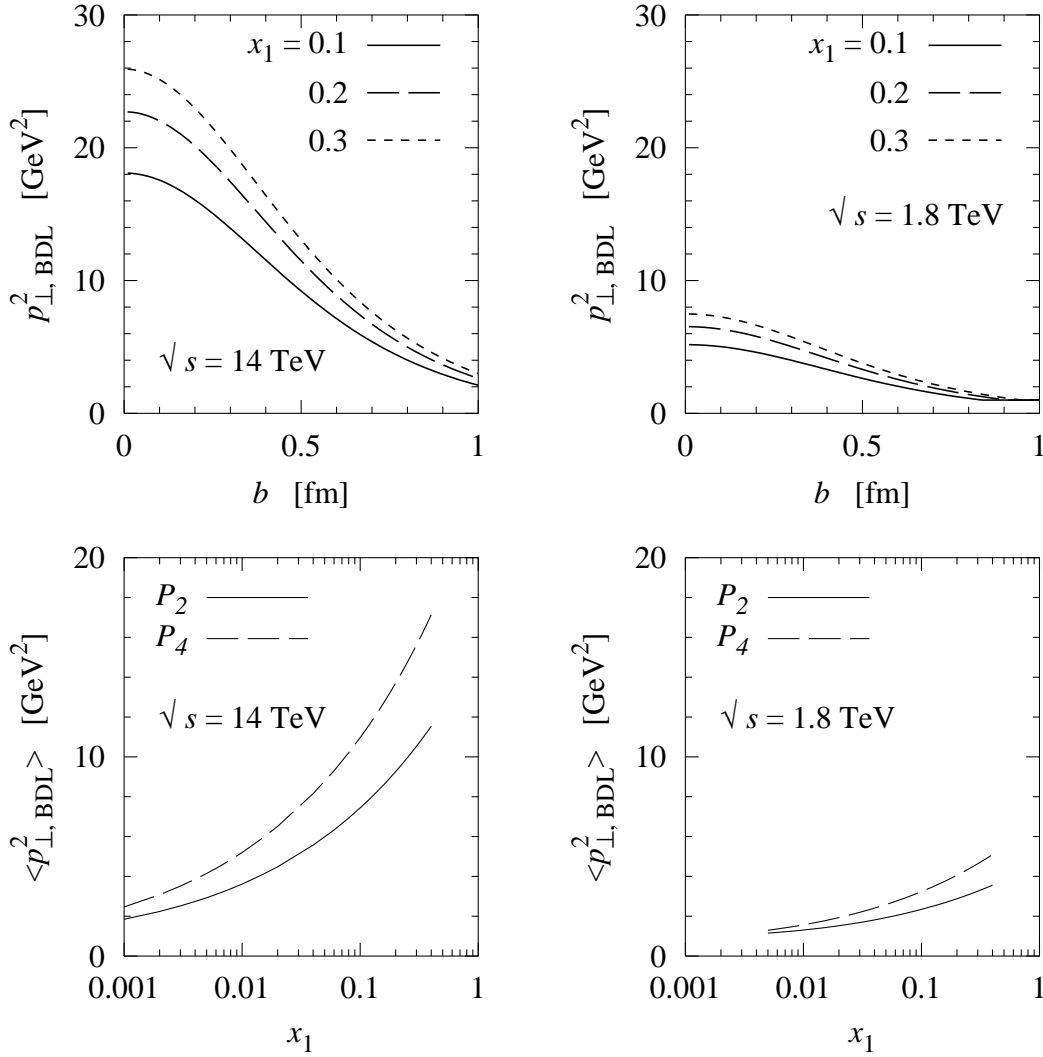


Figure 18: *Upper row*: The transverse momentum squared, $p_{\perp, \text{BDL}}^2$, acquired by a leading gluon (momentum fraction x_1) through interactions with the small- x_2 gluon field in the other proton near the BDL, as a function of the impact parameter of the pp collision, b . Shown are the estimates for LHC (left panel) and Tevatron energies (right panel). *Lower row*: Average values of $p_{\perp, \text{BDL}}^2$ in pp collisions with a single hard process (impact parameter distribution P_2) and two hard processes (distribution P_4), cf. Fig. 15. For leading quarks, the values of $\langle p_{\perp, \text{BDL}}^2 \rangle$ are about half of those for gluons shown here.

0.75, reasonably close to unity. We then determine the maximum p_{\perp} for which the criterion is satisfied. Fig. 17 shows the result for $p_{\perp, \text{BDL}}^2$ for a leading gluon, as a function of the gluon momentum fraction, x_1 ; for leading quarks, the result for $p_{\perp, \text{BDL}}^2$ is approximately 0.5 times the value for gluons. The numerical estimates show that leading partons indeed receive substantial transverse momenta when traversing the small- x_2 gluon medium of the nucleus. We emphasize that our estimate of $p_{\perp, \text{BDL}}$ applies equally well to the interaction of leading partons in the central region of AA collisions.

Turning now to pp collisions, we have to take into account the transverse spatial structure

of the colliding hadrons. A crucial point is that high-energy interactions do not significantly change the transverse position of the leading partons, so that their interaction with the small- x_2 gluons is primarily determined by the gluon density at this transverse position. Because the leading partons in the “projectile” proton are concentrated in a small transverse area, and the small- x_2 gluon density in the “target” proton decreases with transverse distance from the center, it is clear that the maximum transverse momentum for interactions close to the BDL, $p_{\perp,\text{BDL}}^2$, decreases with the impact parameter of the pp collision, b . Fig. 18 (upper row) shows the dependence of $p_{\perp,\text{BDL}}^2$ on b , as obtained with the parametrization of the transverse spatial distribution of gluons based on analysis of the HERA exclusive data, see Section 4.4 [73]. One sees that $p_{\perp,\text{BDL}} \sim$ several GeV in central collisions at LHC. Substantially smaller values are obtained at the Tevatron energy.

To determine the typical transverse momenta of leading partons in events with new particle (or hard dijet) production, we need to average the results for $p_{\perp,\text{BDL}}^2$ over pp impact parameters, with the distribution implied by the hard production process, $P_2(b)$, Eq. (37), or, in the case of four jet production, with $P_4(b)$, Eq. (38). The resulting average values of $p_{\perp,\text{BDL}}^2$ are shown in Fig. 18 (lower row). We find that the suppression of large impact parameters implied by the hard process, described in Sec. 7.1, is sufficient to keep $p_{\perp,\text{BDL}}$ above 1 GeV in more than 99% of events at LHC.

To summarize, our estimates show that in generic central pA and central (triggered) pp collisions at LHC the leading partons acquire substantial transverse momenta due to interactions near the BDL. A much weaker effect is found at the Tevatron energy. The origin of this difference is the increase in the gluon density due to the decrease of x_2 between Tevatron and LHC energies, *cf.* Eq. (39).

7.3 Final state properties in central pp collisions at LHC

The approach to the BDL in the interaction of leading partons implies certain qualitative changes in the hadronic final state in central pp and pA collisions. In particular, these effects will profoundly influence the strong interaction environment for the production of new heavy particles (Higgs boson, *etc.*) at LHC.

The main effect of the BDL is that the leading partons in the projectile acquire substantial transverse momenta, of the order $p_{\perp,\text{BDL}}^2$, when propagating through the dense medium of small- x_2 gluons in the target. As a result, the projectile becomes “shattered”: The leading partons lose coherence and fragment independently over a wide range of rapidities close to the maximal rapidity, corresponding to hadron momentum fractions $z \sim x_1\mu/p_{\perp,\text{BDL}}$ (μ is a typical hadronic mass scale). The differential multiplicity of leading hadrons, integrated over p_{\perp} , is approximately given by the convolution of the nucleon parton density, f_a , with the corresponding parton fragmentation function, $D_{h/a}$, at the scale $Q_{\text{eff}}^2 = 4p_{\perp,\text{BDL}}^2$,

$$\frac{1}{N} \left(\frac{dN}{dz} \right)^{pp \rightarrow h+X} = \sum_{a=q,g} \int dx_1 x_1 f_a(x_1, Q_{\text{eff}}^2) D_{h/a}(z/x_1, Q_{\text{eff}}^2), \quad (41)$$

where N is total number of inelastic events [113, 106, 114]. This corresponds to a very strong suppression of forward hadron production as compared to generic inelastic pp events. The suppression is particularly pronounced for nucleons; one expects that for $z \geq 0.1$ the differential

multiplicity of pions should exceed that of nucleons. At the same time the transverse spectrum of the leading hadrons will be much broader, extending up to $p_{\perp, \text{BDL}} \gg 1 \text{ GeV}$. Finally, the independent fragmentation mechanism implies that there will be no correlations between the transverse momenta of leading hadrons (some correlations will remain, however, because two partons produced in collisions of large- x_1 and small- x_2 partons may end up at similar rapidities).

In central pp collisions at LHC, where leading particles are suppressed in both the forward and backward direction, one expects a large fraction of events with no particles with $z \geq 0.02 - 0.05$ in both fragmentation regions. This amounts to the appearance of long-range rapidity correlations. Such events should show a large energy release at rapidities $y = 4 - 6$. However, similar to the case of diffractive processes in ep scattering (*cf.* the discussion in Section 8), one should expect that there is a $\sim 10\%$ probability for dijets to be produced in pp collisions at large impact parameters without additional interactions between the constituents of the nucleons.

Another important effect of the BDL is a significantly increased energy loss of the leading partons, due to the larger probability of inelastic collisions, and the wider distribution of the propagating parton (dipole) over transverse momenta. In particular, a 2% energy loss would explain the suppression of forward pion production in deuteron-nucleus collisions at RHIC at $p_{\perp} \sim 4 \text{ GeV}$ [99]. Studies of this effect would be possible both at RHIC and LHC, in particular if the forward capabilities of the current detectors were upgraded, as discussed in several proposals presently under consideration. Note that energy loss is neglected in Eq. (41). This corresponds to the usual assumption of models in which parton propagation is treated as multiple elastic rescattering of the parton's accompanying gluon field from the medium. A consistent treatment of energy loss and transverse momentum broadening near the BDL remains a challenge for theory. We note that the pattern of energy loss in our approach is qualitatively different from models in which the leading partons scatter from a classical gluon field (in that case energy loss is negligible) [115].

The approach to the BDL has consequences also for hadron production in the central rapidity region. The multiple scattering of large- x_1 projectile partons from the small- x_2 gluons in the target shifts a large number of these gluons to larger rapidities, leaving numerous “holes” in the target wave function. Furthermore, multiple interactions of partons with moderately small $x_1 \sim x_2$ also occur with large probability. (Unitarity effects should be important for these interactions as well, but have not been studied so far.) Both effects lead to the creation of a substantial amount of color charge, which should result in an increase of soft particle multiplicities over a broad range of rapidities as compared to the situation far from the BDL. This increase should in fact be observable already at Tevatron energies, in central events selected by a trigger on two-jet or Z^0 production. An increase of the multiplicity at rapidities $|y| \leq 1.0$ in such events compared to minimum bias events was indeed reported in Ref. [116]. It would be extremely interesting to extend such studies to higher rapidities.

Our findings imply that new heavy particles at LHC will be produced in a much more “violent” strong-interaction environment than one would expect from the extrapolation of the properties of minimum bias events at the Tevatron. Even the extrapolation of properties of hard dijet events should not be smooth, as the transverse momenta acquired by leading partons are estimated to be substantially larger at LHC than at Tevatron, see Fig. 18.

7.4 Black–disk limit in elastic pp scattering

The assumption of the BDL in the interaction of leading partons, combined with the complex structure of the proton wave function in QCD, allows us to estimate the profile function of the pp elastic amplitude at small impact parameters. This simple estimate nicely explains the observed “blackness” of the phenomenological pp profile function at $b = 0$ at the Tevatron energy, and allows us to extrapolate the profile function at small b to higher energies. It also raises the question whether the observed blackness could be explained on the basis of soft interactions.

In pp collisions at small impact parameters, leading quarks on average receive substantial transverse momenta when passing through the small- x gluon field of the other proton; see Fig. 18. When a single leading quark gets a transverse momentum, p_\perp , the probability for the nucleon to remain intact is approximately given by the square of the nucleon form factor, $F_N^2(p_\perp^2)$, which is ≤ 0.1 for $p_\perp > 1$ GeV, *i.e.*, very small. One may thus conclude that the probability of the survival averaged over p_\perp should be less than 1/2 (on average, half of the time the quark should receive a transverse momentum larger than the average transverse momentum, $p_\perp > 1$ GeV). Because there are six leading quarks (plus a number of leading gluons), the probability for the two protons to stay intact, $|1 - \Gamma^{pp}(s, b)|^2$, *cf.* Eq. (29), should go as a high power of the survival probability for the case of single parton removal, and thus be very small. This crude estimate shows that already at Tevatron energies $|1 - \Gamma^{pp}(s, b = 0)|^2$ should be close to zero owing to hard interactions. The conclusion that the small impact parameter hadron-hadron interactions should become black at high energies follows principally from the composite structure of the hadrons and does not depend on any details. In particular, if taming effects stopped the growth of the dipole–nucleon interaction at a fraction of the BDL, our result would not change. Our conclusion that $\Gamma^{pp}(\sqrt{s} \geq 2 \text{ TeV}, b = 0) \approx 1$ agrees well with the current analysis of the Tevatron data, see *e.g.* Ref. [110].

One can estimate the maximum impact parameter, b_F , up to which hard interactions cause the pp interaction to be “black”. The probability for a leading parton with $x_1 \sim 10^{-1}$ to experience a hard inelastic interaction increases with the collision energy at least as fast as dictated by the increase of the gluon density in the other proton at $x_2 = 4p_\perp^2/(sx_1)$, *cf.* Eq. (39) below. Because $x_2 G(x_2, Q^2) \propto x_2^{-n_h}$ with $n_h \geq 0.2$, the probability should grow as s^{n_h} .⁷ The dipole parametrization of the transverse spatial distribution of gluons, Eq. (22), suggests that the gluon density decreases with the distance from the center of the nucleon approximately as $\sim \exp[-m_g(x_2)\rho]$. If one neglects the transverse spread of the large- x_1 partons as compared to that of the small- x_2 gluons one arrives at an estimate of the energy dependence of b_F as due to hard interactions [102],

$$b_F \approx \frac{n_h \ln(s/s_T)}{m_g(x_2)}, \quad (42)$$

where $\sqrt{s_T} = 2 \text{ TeV}$ is the Tevatron energy. In principle, n_h may decrease at very large virtualities, which would become important at extremely high energies. However, this effect is likely to be compensated by the increased number of constituents in the nucleon wave function affected by the BDL. The above estimate is consistent with the popular Pomeron model parameterization of the pp elastic amplitude [117]. In this model $\Gamma^{pp}(0) \approx 1$ for $s = s_T$ and s-channel

⁷The HERA data on dipole–nucleon scattering suggest that the taming of the gluon density starts only when the probability of inelastic interactions becomes large, $\geq 1/2$. However, for such probabilities of single parton interactions, multiparton interactions ensure that the overall interaction is practically black.

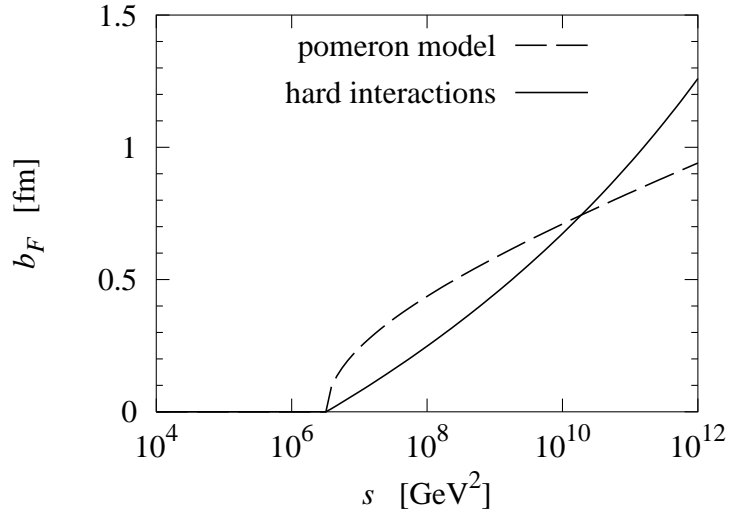


Figure 19: Energy dependence of the maximum impact parameter for “black” pp interactions, b_F . Solid line: Estimate based on the pomeron model fit of pp elastic scattering of [117]. Dashed line: Estimate based on hard interactions, Eq. (42).

unitarity is violated at $b < b_F$ for $s > s_T$. The dependence of b_F on the energy in the Pomeron model is similar to our estimate (42), see Fig. 19. This shows that the two-scale picture of the transverse structure of the nucleon — and the ensuing picture of hard and soft interactions — are self-consistent.

Overall, the analysis of Ref. [102] summarized in this subsection suggests that at high energies hadron-hadron interactions should be “black” in a range of impact parameters growing approximately like $\ln s$, with a coefficient growing only very slowly with energy due to decrease of $m_g(x_2)$ with energy. This corresponds to the Froissart regime, with interactions in the black region dominated by semi-hard interactions, and interactions at large impact parameters dominated by the single Pomeron exchange. At the same time, this analysis indicates that the concept of summing multi-Pomeron exchanges, which should give the dominant contribution at small b , breaks down as the soft physics is gradually squeezed out to large b .

It is worth emphasizing here that, in principle, the BDL can emerge in hadron-hadron interactions already at the level of the soft interactions [118, 119]. However, it is hardly possible to reconcile it with the pre-QCD Feynman parton model description of high energy processes, if one would require it to be valid both in the rest frame of the target and in the center-of-mass frame. Really, within the parton model one cannot generate complete absorption of the projectile in central collisions in the target rest frame, where the target consists of few partons [120]. This puzzle is resolved in QCD, where radiation leads to the “blackening” of the hard interactions at central impact parameters. At extremely high energies, as a result of this effect, all memory of the colliding hadrons is lost. Hence the universal behavior of total cross sections, $\sigma_{\text{tot}} \propto \ln^2(s/s_0)$, with universal coefficient for all hadrons (nuclei) [102].⁸

⁸The increase of the interaction with energy, and the related increase of essential impact parameters, show that the theoretical description of high-energy hadronic collisions should be closer to classical mechanics than to quantum mechanics (V. Gribov, private communication to Yu. Dokshitzer). An example is the cross section for the

7.5 Ion-induced quark-gluon implosion

The small- x phenomena outlined above — the approach to the BDL, and large leading-twist gluon shadowing — play an important role also in the heavy ion collisions at LHC energies. Here we consider just one example, the so-called ion-induced quark-gluon implosion in the nucleus fragmentation region. For a review of other effects in the framework of the color glass condensate model, see Ref. [115].

In generic central AA collisions at collider energies, in analogy to the central pA collisions discussed in Section 7.2, all the leading partons of the individual nucleons are stripped off “soft” partons and form a collection of quarks and gluons with large p_{\perp} . In the rest frame of the fragmenting nucleus, the incoming nucleus has a “pancake” shape with longitudinal length ~ 1 fm for soft partons, and $R_N(m_N/p_N)(x_V/x) \ll R_N$ for hard partons, where $x_V \sim 0.2$ is the average x value for the valence quarks. That is, the nucleons in the nucleus at rest at different locations along the collision axis are hit by the hard partons in the incoming nucleus one after another. In the BDL, no spectators are left. The hit partons are produced with practically the same x that they had in the nucleus (because the fractional energy loss is small), transverse momenta $\sim p_{\perp, \text{BDL}}$, and virtualities $\leq p_{\perp, \text{BDL}}^2$. The partons move in the direction of the projectile nucleus. Because they are emitted at finite angles, their longitudinal velocity is smaller than the speed of light, and they are left behind the projectile wave. However, because the emission angles are small, a shock wave is formed, compressing the produced system in the nucleus rest frame. In the frame co-moving with the shock wave, valence quarks and gluons are streaming in the opposite directions. The resulting pattern of fragmentation of the colliding nuclei leads to an “implosion” of the quark and gluon constituents of the nuclei. The non-equilibrium state produced at the initial stage in the nucleus fragmentation region is estimated to have densities $\propto p_{\perp, \text{BDL}}^2$, which is $\geq 50 \text{ GeV}/\text{fm}^3$ at LHC, and probably $\geq 10 \text{ GeV}/\text{fm}^3$ at RHIC. It seems likely that the partons would rescatter strongly at the second stage, although much more detailed modeling is required to find out whether the system would reach thermal equilibrium. Such large-angle rescattering of partons would lead to production of partons at higher rapidities, and re-population of the cool region. In particular, two gluons from the pancake could have the right energies to produce near-threshold $c\bar{c}$ pairs and χ_c -mesons with small transverse momenta and $x_F(c\bar{c}) \sim 2x_g \sim 0.1$.

7.6 Cosmic ray physics near the GZK cutoff

An extensive program of studies of cosmic rays at energies close to the Greisen-Zatsepin-Kuzmin (GZK) cutoff [10], $E_{\text{GZK}} \simeq 6 \times 10^{10} \text{ GeV}$, is under way, using several cosmic ray detectors. These experiments detect cosmic rays indirectly, via the air showers induced when they enter the atmosphere. The properties of the primary particle need to be inferred from those of the observed shower. For this, a good understanding of the physics of high-energy interactions in the atmosphere is mandatory. The observed characteristics of the shower are predominantly sensitive to leading hadron production ($x_F \geq 10^{-2}$), which, according to our

scattering of a high-energy particle from a potential rapidly decreasing with impact parameter. The essential impact parameters — and therefore the cross section — are infinite within classical mechanics, but finite in quantum mechanics, while they increase with energy in QCD.

discussion above, at these energies probes small- x dynamics down to $x \sim 10^{-10}$, deep inside the regime affected by the approach to the BDL. First studies of these effects were performed in Ref. [121]. It was found that the steeper x_F -distribution of leading hadrons as compared to low-energy collisions, caused by the strong increase of the gluon densities at small x (see Section 7.4), leads to a reduction of the position of the shower maximum, X_{\max} . Account of this effect in the models currently used for the interpretation of the data may shift fits of the composition of the cosmic ray spectrum near the GZK cutoff towards lighter elements. Also, it appears that the present data on $X_{\max}(E)$ exclude the possibility that the prediction of a rapid growth of the critical x -value where the BDL becomes effective ($\sim 1/x^{0.3}$), which is compatible with RHIC and HERA data, would persist up to the GZK cutoff energy.

8 Hard diffraction at hadron colliders

8.1 Diffractive proton dissociation into three jets

LHC will offer an opportunity to study a variety of hard diffractive processes in pp and pA scattering. One interesting aspect of such processes is that they allow to probe rare small-size configurations in the nucleon wave function. A proton in such a configuration can scatter elastically off the target and fragment into three jets, corresponding to the process

$$p + p(A) \rightarrow \text{jet1} + \text{jet2} + \text{jet3} + p(A). \quad (43)$$

The cross section for the diffractive process (43) can be evaluated based on the kind of QCD factorization theorem derived in Ref. [19]. The cross section is proportional to the square of the gluon density in the nucleon at $x \approx M^2(3 \text{ jets})/s$, and virtuality $Q^2 \sim (1 - 2)p_{\perp}^2$ [122]. The distribution over the fractions of the proton longitudinal momentum carried by the jets is proportional to the square of the light-cone wave function of the $|qqq\rangle$ configuration. The numerical estimates suggest [123] that the process could be observed at the LHC energies provided one would be able to measure jets with $p_{\perp} \sim 10$ GeV at very high rapidities, $y_{\text{jet}}(p_{\perp} = 10 \text{ GeV}) \sim 6$, and with a large background from leading-twist hard diffraction. The latter will be suppressed in pA collisions, because the coherent 3-jet process has a much stronger A -dependence than the background due to soft and hard diffraction induced by strong interactions. The main background will be due to hard electromagnetic interactions of the proton with the Coulomb field of the nucleus. We note that the discussed mechanism of hard diffraction requires that the interaction of the spatially small three-quark color singlet configuration with the proton be far from the BDL at small impact parameters. Otherwise production at small impact parameters would be suppressed, leading to a dip in the t -dependence of the differential cross section for the production of three jets with moderate p_{\perp} .

The detection of the three-jet final state produced by diffractive scattering of a qqq configuration from a proton should be easier than that resulting from e^+e^- annihilation into $q\bar{q}g$, as in the former case all color charges are in the triplet representation, leading to less radiation between the jets. Finally, it would also be possible to study the process $pp \rightarrow pn + \text{two jets}$, which is similar to pion dissociation into two jets. Experimentally, this would require the measurement of jets at rapidities $y \sim 4$, together with the detection of a leading neutron by a zero-degree calorimeter, as is present in several of the LHC detectors (ALICE, ATLAS, CMS).

8.2 Exclusive diffractive Higgs production

Hard diffractive processes are also being considered in connection with the production of new heavy particles in pp collisions at LHC. In particular, the exclusive diffractive production of Higgs bosons,

$$p + p \rightarrow p + (\text{rapidity gap}) + H + (\text{rapidity gap}) + p, \quad (44)$$

is regarded as a promising candidate for the Higgs search; see Ref. [124] and references therein. From the point of view of strong interactions, this process involves a delicate interplay between “hard” and “soft” interactions, which can be described within our two-scale picture of the transverse structure of the nucleon [112]. The Higgs boson is produced in a hard partonic process, involving the exchange of two hard gluons between the nucleons. The impact parameter distribution of the cross section for this process is described by the square of the convolution of the transverse spatial distributions of gluons in the in and out states, $P_4(b)$, defined in Eq. (38), where the scale is of the order of the gluon transverse momentum squared, $\sim M_H^2/4$. In addition, the soft interactions between the the spectator systems have to conspire in such a way as not to fill the rapidity gaps left open by the hard process. The probability for this to happen is approximately given by one minus the probability of an inelastic pp interaction at a given impact parameter, or $|1 - \Gamma^{pp}(s, b)|^2$. The product of the two probabilities, which determines the b -distribution for the total process, is shown in Fig. 20a. At small b the probability for no inelastic interaction is very small $|1 - \Gamma^{pp}|^2 \approx 0$, leading to a strong suppression of small b in the overall distribution.

The so-called rapidity gap survival probability, which measures the “price” to be paid for leaving the protons intact, is given by the integral [112]

$$S^2 \equiv \int d^2b |1 - \Gamma^{pp}(s, b)|^2 P_4(b). \quad (45)$$

Fig. 20b shows our result for this quantity, with s ranging between Tevatron and LHC energies, for various values of the dipole mass in the two-gluon form factor of the nucleon, m_g^2 , Eq. (22). The survival probability decreases with s because the size of the “black” region at small impact parameters (in which inelastic interactions happen with high probability) grows with the collision energy. Note that the effective x values in the gluon distribution decrease with the energy (for fixed mass of the produced Higgs boson), resulting in smaller effective values of m_g^2 . This makes the actual drop of the survival probability with energy slower than appears from the fixed- m_g^2 curves of Fig. 20b. Our estimates of S^2 are in reasonable agreement with those obtained by Khoze et al. [125] in a multi-Pomeron model, as well as with those reported by Maor et al. [126]. In view of the different theoretical input to these approaches this is very encouraging.

Our results for the rapidity gap survival probability apply equally well to the production of two hard dijets instead of a Higgs boson. For this process, one expects much larger cross section, and it would be possible to investigate experimentally the interplay of hard physics and absorptive effects, which leads to a rich, distinctive structure of the cross section as a function of the transverse momenta of the two protons, $\Delta_{1\perp}$ and $\Delta_{2\perp}$ [127]. This structure should also rather strongly depend on the rapidities of the jets, due to the x -dependence of the transverse spatial distribution of gluons, see Sec. 4.4 (L. Frankfurt *et al.*, in preparation).

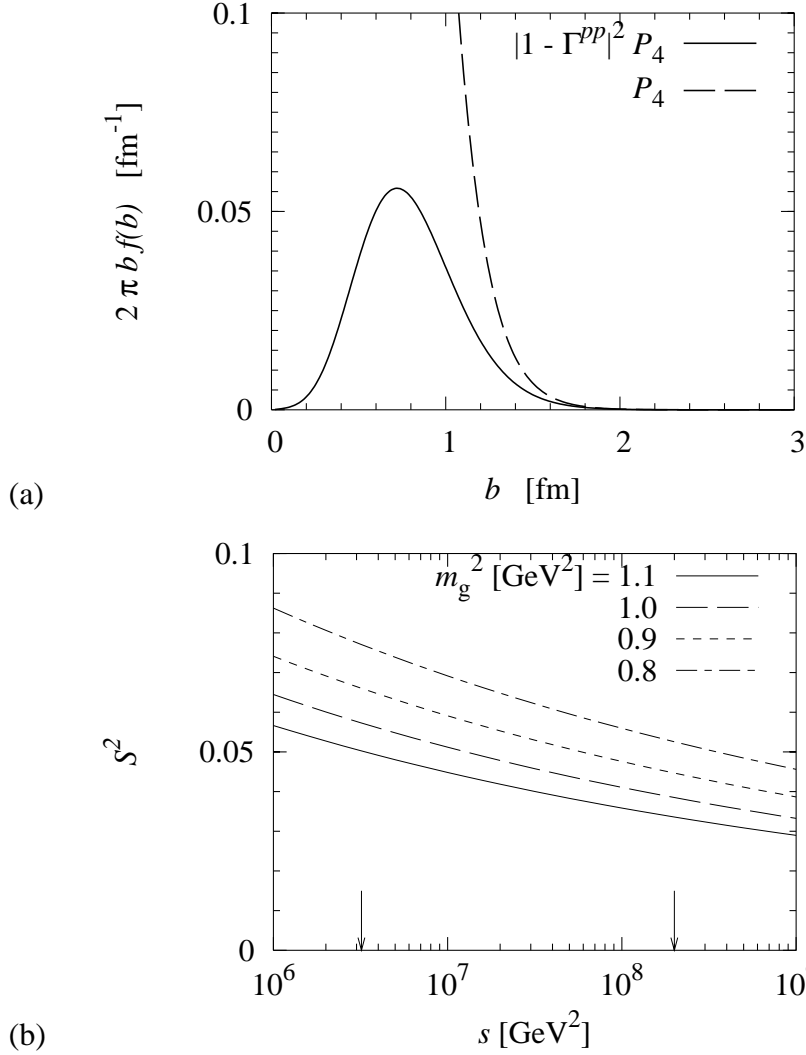


Figure 20: (a) The impact parameter (b -) distribution of the cross section for diffractive Higgs production at LHC ($\sqrt{s} = 14$ TeV). Dashed line: b -distribution of the hard process, $P_4(b)$, Eq. (38), *cf.* Fig. 15. Solid line: b -distribution of the total process, $|1 - \Gamma^{pp}(s, b)|^2 P_4(b)$. Here, $m_g^2 = 1$ GeV². (b) The rapidity gap survival probability, S^2 , Eq. (45) [112]. Shown is the result as a function of s , for various values of the mass parameter in the two-gluon form factor, m_g^2 . The Tevatron and LHC energies are marked by arrows.

8.3 Inclusive hard diffractive processes

Inclusive hard diffractive processes, such as

$$\begin{aligned}
 p + p &\rightarrow p + (\text{rapidity gap}) + 2 \text{ jets} + X, \\
 p + p &\rightarrow p + (\text{rapidity gap}) + 2 \text{ jets} + X + (\text{rapidity gap}) + p,
 \end{aligned}
 \tag{46}$$

offer a possibility to probe the “periphery” of the proton with hard scattering processes. The cross section for these processes is again suppressed compared to the naive estimate based on the diffractive parton densities of the proton measured in ep scattering at HERA. As in the case

of exclusive diffractive Higgs production, the cause of this is the very small probability for the nucleons not to interact inelastically at small impact parameters. The suppression factors can be estimated by generalizing the approach to the description of hard and soft interactions outlined in Sec. 8.2. Simple estimates along the lines of Eq. (45) naturally reproduce the suppression factors of the order $0.1 - 0.2$ observed at Tevatron. However, the results in this case are more sensitive to the details of the impact parameter dependence of the hard scattering process and the soft spectator interactions.

Measurements of inclusive hard diffractive processes at LHC would allow one to perform many interesting tests of the diffractive reaction mechanism. In particular, one could (*a*) investigate how the overall increase of the nucleon size with energy leads to a suppression of hard diffraction, (*b*) check how the rate of suppression depends on the x -value of the parton involved in the hard process, (*c*) look for the breakdown of Regge factorization, that is, the change of the diffractive parton distributions with $x_{\mathbb{P}}$.

9 Summary and Outlook

9.1 From HERA to LHC

The HERA experiments and the theoretical investigations they stimulated have greatly advanced our knowledge of small- x dynamics. The key result of these studies are: (*a*) The rapid increase with energy of the cross section for the scattering of small $q\bar{q}$ wave packets from the nucleon. HERA energies are not sufficient to reach the BDL in the dipole-nucleon interaction in average configurations. The interaction of gluon dipoles in diffractive scattering appears to be close to the unitarity limit for $Q^2 \sim 4 \text{ GeV}^2$, but this can hardly be verified directly because of the lack of a trigger for such configurations. (*b*) The establishment of a three-dimensional picture of the partonic structure of the nucleon. The leading partons are concentrated in a much smaller transverse area than the area associated with the nucleon in soft hadronic processes at high energies.

We have demonstrated that these elements of small- x dynamics are of utmost importance for building a realistic description of pp/pA collisions at LHC. The BDL will be commonplace in central pp/pA collisions at LHC, affecting average configurations in the colliding protons (nuclei), with numerous consequences for the hadronic final state. In particular, these phenomena qualitatively change the strong interaction environment for new particle production.

We have identified several directions for future theoretical research, necessary for describing the expected new phenomena at LHC. These include the resummation approaches to QCD radiation (combining logarithms of Q^2 and $1/x$), the account for energy loss in the interaction of leading partons with the small- x gluon medium, and the development of realistic models of hadron production in central pp/pA collisions with interactions close to the BDL.

An overarching goal of future theoretical research on the structure of the nucleon and small- x dynamics should be to bring together the approaches starting from “soft” (hadronic) and “hard” (partonic) physics, as envisioned in Gribov’s space-time picture of high-energy interactions. We have pointed out several instances in which “soft” and “hard” dynamics match

smoothly or exhibit a delicate interplay, *e.g.* pp elastic scattering at small impact parameters, or diffractive processes.

A natural question is what are the most promising directions for future experimental studies of small- x dynamics. This question needs to be discussed with regard to the general long-term perspectives in high-energy physics. We assume here that the decision by the DESY management to stop HERA operations in 2007 will be enacted. This would clearly be a great loss, as many insights could be obtained from further measurements at HERA in both ep and eA mode, see *e.g.* the proposals put forward for the HERA III run. We shall thus focus on the possibilities offered by LHC, with comments on the possible future program at Tevatron, as well as on the electron-ion collider envisaged in the U.S. government's long-range plan [128]. The small- x investigations at LHC described in the following subsections are meant to complement the studies of central inelastic pp/pA collisions (Sec. 7.4) and diffractive phenomena in pp/pA scattering, which are the main topic of this review.

9.2 Measurement of parton densities in pp and pA collisions at LHC

Measurements at LHC could greatly expand the x -range in which the parton densities are known. This would require measurements of hard processes such as

$$\begin{array}{ll}
 pp \rightarrow \text{jet1} + \text{jet2} + X & \text{dijet production} \\
 \text{jet} + \gamma + X, \gamma + \gamma + X & \text{photon production} \\
 Q + \bar{Q} + X & \text{heavy quark production} \\
 l^+ + l^- + X & \text{Drell-Yan pair production} \\
 W^\pm(Z) + X & \text{weak boson production,}
 \end{array} \tag{47}$$

in the region where one of the colliding partons carries small momentum fraction. The cross sections of all these processes remain large down to the very edge of the LHC kinematics, corresponding to $x \approx 3 \times 10^{-7}$ for Drell-Yan pair production with $M_{\mu^+\mu^-} = 5 \text{ GeV}$ [129, 123]. The main limitations come from the need to identify relatively low- p_\perp jets, and from the detector acceptance. The smaller the x one wants to probe, the more forward one must look, as the momentum fractions of colliding partons are related to the rapidities of the produced jets as

$$x_{1,2} = \frac{p_\perp}{\sqrt{s}} (e^{\pm y_1} + e^{y_2}). \tag{48}$$

The presently planned configuration of the CMS detector would allow for the measurement of dijet production down to $x \approx 3 \times 10^{-6}$ at $p_\perp = 10 \text{ GeV}$. This would push parton distribution measurements deep into the region where unitarity effects play an important role in the dynamics of hard processes, and where evolution effect in both $\ln(1/x)$ and $\ln Q^2$ need to be taken into account. When the BDL is reached, the M^2 -dependence of the cross section, $d\sigma/dx_1 dx_2$, is predicted to be much slower than $\propto 1/M^2$ as in the leading twist approximation, similarly to the case of the inclusive deep inelastic scattering [130].

If several of the reactions (47) were measured, it would allow for independent tests of the QCD factorization, which may be violated at intermediate virtualities owing to the strong interaction of the propagating system with the small- x gluon medium, see Sec. 7. The latter will be strongly enhanced in the region of x_1 close to 1. These effects, which are of great interest in themselves, can be probed by comparing the production cross sections for fixed, large x_1 and various values of x_2 , including relatively large ones where the parton densities are known.

9.3 Small- x phenomena in ultraperipheral collisions at LHC

It has been long known that nuclei in high-energy collisions generate a large flux of equivalent photons, which are spread in the transverse plane over distances substantially larger than twice the nuclear radius — the maximal distance at which strong interactions are possible. Scattering processes induced by these photons are referred to as ultraperipheral collisions. They have a distinctive signature, which allows them to be separated from the more frequent events caused by strong interactions. Experimentally, one selects events in which one of the nuclei remains intact, or emits one or a few neutrons by way of dipole excitation. Such events are extremely rare in scattering at impact parameters smaller than twice the nuclear radius.

The experiments at HERA have shown that photon-induced processes provide a well-understood probe of the gluon density in the proton. At LHC, such processes could be studied up to invariant γp energies (*i.e.*, γA energies per nucleon) exceeding the maximal HERA energy by a factor of 10. This would allow one to use dijet (charm, *etc.*) production to measure the gluon density in the proton/nucleus down to $x \approx 3 \times 10^{-5}$ for $p_{\perp} \sim \text{few GeV}$ [131, 132], as well as the diffractive gluon density. Among other things, measurements of diffractive channels would allow one to perform critical tests of the HERA observation of a large probability of gluon-induced diffraction (see Sec. 5), and the prediction of its further enhancement for nuclear targets, see Ref. [109] and references therein. Another important measurement would be the t -dependence of gluon-induced diffraction and its change with energy, using CMS-TOTEM in pA mode. We remind the reader that the lack of direct information on the t -dependence of diffraction leads to a large uncertainty in the predictions for leading-twist nuclear shadowing (see Sec. 5.3).

Ultraperipheral collisions would also allow one to study the coherent production of heavy quarkonia, $\gamma A \rightarrow J/\psi (\Upsilon) + A$ at $x \leq 10^{-2}$, and to investigate the propagation of small dipoles through the nuclear medium at high energies. The QCD factorization theorem predicts that the A -dependence of the amplitude for this process should change between the color transparency regime (observed at FNAL [77]), where it is $\propto A$, and the perturbative color opacity regime, where it is proportional to the leading-twist shadowed gluon density. It would be possible also to use coherent diffraction from nuclei to study the approach to the BDL in $\gamma A \rightarrow X + A$, by comparing the measured cross section to the BDL prediction, *cf.* Sec. 6.4. The most promising channels are J/ψ and dijet photoproduction; see Ref. [133] for a review and discussion. In AA collisions, it is difficult to separate processes induced by the photons generated by the left- and right-moving nucleus. Away from zero rapidity, a low-energy contribution tends to dominate, limiting the range of x which could be explored for production of a state with mass M to $x \geq MA/(2p_A)$, where p_A is the momentum of the colliding nuclei. However, it seems that selection of events in which the heavy nucleus undergoes a dipole excitation enhances the contribution of hard photons [134], allowing one to extend the x -range of the measurements (by a factor of up to 10 in the case of J/ψ production). The challenge is to trigger both on events with and without break-up. In pA mode, the dominant process will be the production of heavy quarkonia. Such measurements would extend the W -range of the HERA measurements by a factor of three, and make it possible to measure directly the t -dependence of the cross section in a very broad range of rapidities, using the proposed 420m proton tagger [135], which is critical for a more accurate determination of the x -dependence of the nucleon's transverse structure, see Sec. 4.4. Note also that in pp scattering it is possible to detect protons at very

small momentum transfers, where Coulomb exchange dominates [136]. This would allow one to measure exclusive photoproduction of heavy quarkonia in pp scattering with good statistics [137, 138].

9.4 Small- x physics at RHIC and an electron-ion collider

The LHC measurements described in Sections 9.2 and 9.3 will probe small- x dynamics at least down to $x \sim 10^{-5}$. However, most of these measurements are restricted to scales $Q \geq 5$ GeV, and it would be difficult to connect them with the physics at smaller scales (virtualities), $Q \sim 2 - 3$ GeV, relevant for the overall structure of central pp/pA collisions at LHC (see Sec. 7). The gap could be filled, to some extent, by experiments at RHIC and the proposed electron-ion collider [128, 139].

Extension of the forward acceptance of the current RHIC detectors would make it possible to measure Drell-Yan pair production at $x \sim 10^{-3}$ in pp and pA/dA scattering. This would allow one to test the predictions for leading-twist nuclear shadowing and look for deviations from the leading-twist prediction in the p_{\perp} distributions of the dileptons. Qualitatively, one expects a suppression of the low transverse momentum part of the distribution up to $p_{\perp} \sim p_{\perp, \text{BDL}}$. As mentioned above, such measurements would also allow one to probe the role of final state interactions by varying the x -values of the leading partons in the proton. If absorption effects were significant, one would have to introduce a cut on $x_p \leq 0.3$ to suppress these effects, which would reduce somewhat the x_A -range where the parton densities can be probed.

The eRHIC design for a future electron-ion collider envisages an ep/eA collider with $\sqrt{s} \leq 100$ GeV, with significantly higher luminosity than HERA, and the ability to continuously vary the beam energies over a wide range [128, 139]. With such a facility one could systematically study a variety of color transparency phenomena and use them to disentangle the quark-gluon structure of hadrons and nuclei; one could also measure longitudinal cross sections, which provide stringent tests of the range of the validity of the leading-twist approximation at small x (see Sections 3, 4 and 5). In eA collisions, one could study the transition of the nonperturbative shadowing at low Q^2 to the regime of leading-twist shadowing at high Q^2 , and explore whether there exists an “intermediate” regime characterized by weak coupling but large parton densities. The ability to perform such measurements with a range of nuclear beams would allow one to study these effects as a function of the nuclear thickness, reaching values 1.5 times larger than the average thickness of the heavy nuclei. No other planned facilities would be able to cover this important kinematic region. Finally, eRHIC would make it possible to measure the t -dependence of a variety of hard exclusive processes in a wide range of x , $0.1 > x \geq 0.003$. This would probe the transverse structure of the proton directly in the x -range relevant for understanding nucleon fragmentation in central pp/pA collisions at LHC.

Acknowledgments. We would like to thank our colleagues, many of them collaborators of many years, for their contributions to the studies discussed in this review and many enjoyable discussions, in particular H. Abramowicz, J. Bjorken, S. Brodsky, J. Collins, J. Dainton, Yu. Dokshitzer, A. DeRoeck, H. Drescher, A. Dumitru, K. Eggert, A. Freund, V. Gribov, V. Guzey, A. Levy, L. Lipatov, M. McDermott, G. Miller, A. Mueller, A. Radyushkin, T. Rogers,

W. Vogelsang, R. Vogt, H. Weigert, S. White, and M. Zhalov. This work is supported by U.S. Department of Energy Contract DE-AC05-84ER40150, under which the Southeastern Universities Research Association (SURA) operates the Thomas Jefferson National Accelerator Facility. L. F. and M. S. acknowledge support by the Binational Scientific Foundation. The research of M. S. was supported by DOE. M.S. thanks the Frankfurt Institute for Advanced Studies at Frankfurt University for the hospitality during the time when this work was completed.

References

- [1] Gribov VN. *JETP Lett.* 41:667 (1961)
- [2] Gribov VN. arXiv:hep-ph/0006158.
- [3] Froissart M. *Phys. Rev.* 123:1053 (1961)
- [4] Gross DJ, Wilczek F. *Phys. Rev. Lett.* 30:1343 (1973)
- [5] Politzer HD, *Phys. Rev. Lett.* 30:1346 (1973)
- [6] Bjorken JD. *Phys. Rev.* 179: 1547 (1969)
- [7] Feynman RP. *Phys. Rev. Lett.* 23:1415 (1969)
- [8] Gross DJ, Wilczek F. *Phys. Rev. D* 8:3633 (1973); *ibid D* 9:980 (1974)
- [9] Dokshitzer YL. *Sov. Phys. JETP* 46:641 (1977)
- [10] Greisen K. *Phys. Rev. Lett.* 16: 748 (1966); Zatsepin GT, Kuzmin VA. *JETP Lett.* 4:78 (1966)
- [11] Gribov VN, Lipatov LN. *Sov. J. Nucl. Phys.* 15: 438 (1972); Lipatov LN. *Sov. J. Nucl. Phys.* 20: 94 (1975)
- [12] Altarelli A, Parisi G. *Nucl. Phys. B* 126:298 (1977)
- [13] Ellis RK, Furmanski W, Petronzio R. *Nucl. Phys.* B207:1 (1982); *ibid.* B212:29 (1983)
- [14] Ciafaloni M. *Nucl. Phys. B* 296:49 (1988); Catani S, Fiorani F, Marchesini G. *Phys. Lett. B* 234:339 (1990)
- [15] Blaettel B, Baym G, Frankfurt L, Strikman M. *Phys. Rev. Lett.* 70:896 (1993).
- [16] Frankfurt L, Miller GA, Strikman M. *Phys. Lett. B* 304:1 (1993)
- [17] Frankfurt L, Radyushkin A, Strikman M. *Phys. Rev. D* 55:98 (1997)
- [18] Miettinen HI, Pumplin J. *Phys. Rev. D* 18:1696 (1978)
- [19] Frankfurt L, Miller GA, Strikman M. *Phys. Rev. D* 65: 094015 (2002)
- [20] Gribov VN. *The Theory of complex angular momenta: Gribov lectures on theoretical physics.* Cambridge: Cambridge Univ. Press (2003)
- [21] Brodsky SJ, *et al.* *Phys. Rev. D* 50:3134 (1994)
- [22] Cooper–Sarkar AM, Devenish RCE, De Roeck A. *Int. J. Mod. Phys. A* 13:3385 (1998)
- [23] Gabareen Mokhtar A. (H1 Collab.) arXiv:hep-ex/0406036
- [24] Gluck M, Reya E, Vogt A. *Z. Phys. C* 67:433 (1995)

- [25] Cheng H, Wu TT. *Phys. Rev. D* 186:1611 (1969)
- [26] Frankfurt L, Koepf W, Strikman M. *Phys. Rev. D* 54:3194 (1996)
- [27] Low FE. *Phys. Rev. D* 12:163 (1975)
- [28] Nussinov S. *Phys. Rev. Lett.* 34:1286 (1975)
- [29] Gunion J, Soper D. *Phys. Rev. D* 15:2617 (1977)
- [30] McDermott M, Frankfurt L, Guzey V, Strikman M. *Eur. Phys. J. C* 16:641 (2000)
- [31] Diakonov D. *Prog. Part. Nucl. Phys.* 51:173 (2003)
- [32] Mueller AH. *Nucl. Phys. B* 335:115 (1990)
- [33] Frankfurt L, Guzey V, Strikman M. *J. Phys. G* 27: R23(2001)
- [34] Frankfurt L, Sherman VE. *Sov. J. Nucl. Phys.* 23:581 (1976)
- [35] Lipatov LN. *Sov. J. Nucl. Phys.* 23:338 (1976)
- [36] Kuraev EA, Lipatov LN, Fadin VS. *Sov. Phys. JETP* 44:443 (1976); *ibid.* 45:199 (1977); Balitsky II, Lipatov LN. *Sov. J. Nucl. Phys.* 28:822 (1978)
- [37] Ciafaloni M, Camici G. *Phys. Lett. B* 430:349 (1998); Ciafaloni M, Colferai D. *Phys. Lett. B* 452:372 (1999)
- [38] Fadin VS, Lipatov LN. *Phys. Lett. B* 429:127 (1998)
- [39] Ciafaloni M, Colferai D, Salam GP, Stasto AM, *Phys. Rev. D* 68:114003 (2003)
- [40] Altarelli G, Ball RB, Forte S. *Nucl. Phys. B* 674:459 (2003)
- [41] Ciafaloni M, Colferai D, Salam GP, Stasto AM. *Phys. Lett. B* 587:87 (2004)
- [42] Bartels J, Loewe M. *Z. Phys. C* 12:263 (1982)
- [43] Muller D, *et al.* *Fortsch. Phys.* 42:101 (1994)
- [44] Abramowicz H, Frankfurt L, Strikman M. *Surveys High Energ. Phys.* 11:51 (1997); also in: SLAC Summer Inst. 1994:0539
- [45] Ji XD. *Phys. Rev. D* 55:7114 (1997)
- [46] Radyushkin A. *Phys. Rev. D* 56: 5524 (1997)
- [47] Frankfurt L, Freund A, Strikman M. *Phys. Rev. D* 58:114001 (1998); Erratum. *Phys. Rev. D* 59:119901 (1999)
- [48] Collins JJ, Freund A. *Phys. Rev. D* 59: 074009 (1999)
- [49] Collins JC, Frankfurt L, Strikman M. *Phys. Rev. D* 56:2982 (1997)

- [50] Diehl M. *Phys. Rept.* 388:41 (2003)
- [51] Belitsky AV, Radyushkin AV. arXiv:hep-ph/0504030
- [52] Frankfurt L, Freund A, Guzey V, Strikman M. *Phys. Lett.* B418:345(1998); Erratum. *Phys. Lett.* B429:14 (1998)
- [53] Shuvaev AG, Golec-Biernat KJ, Martin AD, Ryskin MG. *Phys. Rev. D* 60:014015 (1999)
- [54] Musatov I, Radyushkin A, *Phys. Rev. D* 61:074027 (2000)
- [55] Ryskin MG. *Z. Phys. C* 57:89 (1993)
- [56] Frankfurt L, Koepf W, Strikman M. *Phys. Rev. D* 57:512 (1998)
- [57] Levy, A. *Nucl. Phys. Proc. Suppl.* 146: 92 (2005)
- [58] Martin AD, Ryskin MG, Teubner T. *Phys. Rev. D* 55: 4329 (1997)
- [59] Frankfurt L, McDermott M, Strikman M. *JHEP* 9902:002 (1999)
- [60] Martin AD, Ryskin MG, Teubner T. *Phys. Lett.* B454:339 (1999)
- [61] Brodsky SJ, Close FE, Gunion JF. *Phys. Rev. D* 6:177 (1972)
- [62] McDermott M, Sandapen R, G. Shaw G. *Eur. Phys. J. C* 22:655 (2002)
- [63] Favart L. *Eur. Phys. J.* C33:S509 (2004)
- [64] Freund A, McDermott M. *Eur. Phys. J.* C23:651 (2002)
- [65] Freund A, McDermott M, Strikman M. *Phys. Rev. D* 67:036001 (2003)
- [66] Poblitsa PV. *Phys. Rev. D* 66:094002 (2002)
- [67] Frankfurt L, Strikman M. *Phys. Rev. D* 66:031502 (2002)
- [68] Strikman M, Weiss C. *Proc. XII International Workshop on Deep Inelastic Scattering (DIS 2004), Strbske Pleso, Slovakia, Apr. 14-18, 2004.* (arXiv:hep-ph/0408345)
- [69] Adloff C, *et al.* (H1 Collab.) *Phys. Lett.* B483:23 (2000)
- [70] Chekanov S, *et al.* (ZEUS Collab.) *Nucl. Phys. B* 695:3 (2004)
- [71] Strikman M, Weiss C. *Phys. Rev. D* 69:054012 (2004)
- [72] Frankfurt L, Strikman M. *Nucl. Phys. Proc. Suppl.* 79:671 (1999)
- [73] Frankfurt L, Strikman M, Weiss C. *Phys. Rev. D* 69:114010 (2004)
- [74] Bertsch G, Brodsky SJ, Goldhaber AS, Gunion J. *Phys. Rev. Lett.* 47:297 (1981)
- [75] Frankfurt L. Professor Habilitation thesis, Leningrad Institute for Nuclear Physics, Leningrad (1981)

- [76] Arneodo M. *Phys. Rept.* 240:301 (1994)
- [77] Sokoloff MD, *et al.* *Phys. Rev. Lett.* 57:3003 (1986)
- [78] Aitala EM, *et al.* (E791 Collab.) *Phys. Rev. Lett.* 86:4773 (2001); *ibid.* 86:4768 (2001)
- [79] Trentadue L, Veneziano G. *Phys. Lett.* B323:201 (1994)
- [80] Collins JC. *Phys. Rev. D* 57:3051 (1998); Erratum. *Phys. Rev. D* 61:019902 (2000)
- [81] Ingelman G, Schlein PE. *Phys. Lett. B* 152:256 (1985)
- [82] Frankfurt L, Strikman M. *Eur. Phys. J.* A5:293 (1999)
- [83] Buchmuller W, Gehrmann T, Hebecker A. *Nucl. Phys. B* 537:477 (1999)
- [84] Bartels J, Ellis JR, Kowalski H, Wusthoff M. *Eur. Phys. J.* C7:443 (1999)
- [85] Chekanov S, *et al.* (ZEUS Collab.) *Phys. Lett.* B516:273 (2001)
- [86] Goulianos K. *Phys. Lett.* B358:379 (1995)
- [87] Erhan S, Schlein PE. *Phys. Lett.* B481:177 (2000)
- [88] Gribov VN. *Sov. Phys. JETP* 29:483 (1969)
- [89] Gribov VN. *Sov. Phys. JETP* 30:709 (1970)
- [90] Abramovsky VA, Gribov VN, Kancheli OV. *Sov. J. Nucl. Phys.* 18:308 (1974)
- [91] Treleani D. *Int. J. Mod. Phys.* A11:613 (1996)
- [92] Alvero L, Frankfurt L, Strikman M. *Eur. Phys. J.* A5:97 (1999)
- [93] Frankfurt L, Guzey V, Strikman M. *Phys. Rev. D* 71:054001 (2005)
- [94] Piller G, Weise W. *Phys. Rept.* 330:1 (2000)
- [95] Kaidalov AB. *Phys. Rept.* 50:157 (1979)
- [96] McLerran L. arXiv:hep-ph/0402137.
- [97] Vogt R. *Phys. Rev. C* 71:054902 (2005)
- [98] Jipa A. (BRAHMS Collab.) *Acta Phys. Hung.* A22:121 (2005)
- [99] Guzey V, Strikman M, Vogelsang W. *Phys. Lett. B* **603**, 173 (2004)
- [100] Rogers T, Guzey V, Strikman M, Zu X. *Phys. Rev. D* 69:074011 (2004)
- [101] Pumplin J, *et al.* *JHEP* 0207:012 (2002)
- [102] Frankfurt L, Strikman M, Zhalov M. *Phys. Lett.* B616:59 (2005)
- [103] Golec-Biernat K, Wusthoff M. *Phys. Rev. D* 59:014017 (1999)

- [104] Bondarenko S, Kozlov M, Levin E. *Nucl. Phys.* A727:139 (2003)
- [105] Balitsky I. *Nucl. Phys. B* 463:99 (1996); Kovchegov YV. *Phys. Rev. D* 61:074018 (2000)
- [106] Frankfurt L, Guzey V, McDermott M, Strikman M. *Phys. Rev. Lett.* 87:192301 (2001)
- [107] Munier S, Stasto AM, Mueller AH. *Nucl. Phys.* B603:427 (2001)
- [108] Mueller AH, Qiu JW. *Nucl. Phys.* B268:427 (1986)
- [109] Frankfurt L, Guzey V, Strikman M. *Phys. Lett.* B586:41 (2004)
- [110] Islam MM, Luddy RJ, Prokudin AV. *Mod. Phys. Lett. A* 18:743 (2003)
- [111] Abe F, *et al.* (CDF Collab.) *Phys. Rev. Lett.* 79:584 (1997); *Phys. Rev. D* 56:3811 (1997)
- [112] Frankfurt L, Strikman M, Weiss C. *Ann. Phys. (Leipzig)* 13:665 (2004)
- [113] Berera A, *et al.* *Phys. Lett.* B403:1 (1997)
- [114] Dumitru A, Gerland L, Strikman M. *Phys. Rev. Lett.* 90:092301 (2003); Erratum. *Phys. Rev. Lett.* 91:259901 (2003)
- [115] Venugopalan R. arXiv:hep-ph/0412396.
- [116] Affolder T, *et al.* (CDF Collab.) *Phys. Rev. D* 65:092002 (2002)
- [117] Donnachie A, Landshoff PV. *Phys. Lett.* B296:227 (1992)
- [118] Migdal AA, Polyakov AM, Ter-Martirosian KA. *Phys. Lett.* B48:239 (1974)
- [119] Amati D, Le Bellac M, Marchesini G, Ciafaloni M. *Nucl. Phys.* B112:107 (1976)
- [120] Kancheli OV. arXiv:hep-ph/0008299
- [121] Drescher HJ, Dumitru A, Strikman M. *Phys. Rev. Lett.* 94:231801 (2005)
- [122] Frankfurt L, Strikman M. *Surveys High Energ. Phys.* 14:9 (1999)
- [123] Lippmaa E, *et al.* (FELIX Collab.) SLAC-R-638; CERN-LHCC-97-45, LHCC-I10 (1997); Ageev A, *et al.* *J. Phys. G* 28:R117 (2002)
- [124] Kaidalov AB, Khoze VA, Martin AD, Ryskin MG. *Eur. Phys. J.* C31:387 (2003)
- [125] Khoze VA, Martin AD, Ryskin MG. *Eur. Phys. J.* C18:167 (2000)
- [126] Maor U. Talk presented at the Workshop “HERA and the LHC”, CERN, Geneva, March 26–27, 2004
- [127] Khoze VA, Martin AD, Ryskin MG. *Eur. Phys. J.* C24:581 (2002)
- [128] The Electron Ion Collider White Paper, BNL Rep. BNL-68933 (2002)
- [129] Alvero L, Collins JC, Strikman M, Whitmore JJ. *Phys. Rev. D* 57:4063 (1998)

- [130] Frankfurt L, Strikman M. *Phys. Rev. Lett.* 91:022301 (2003)
- [131] Klein SR, Nystrand J, Vogt R. *Phys. Rev. C* 66:044906 (2002)
- [132] Strikman M, Vogt R, White S. Preprint LBNL-57843 (2005)
- [133] Frankfurt L, Strikman M, Zhalov M. *Acta Phys. Polon.* B34:3215 (2003)
- [134] Baltz AG, Klein SR, Nystrand J. *Phys. Rev. Lett.* 89:012301 (2002)
- [135] Albrow MG, *et al.* CERN Rep. CERN-LHCC-2005-025
- [136] Piotrkowski K. *Proc. Physics at LHC*, in press
- [137] Khoze VA, Martin AD, Ryskin MG. *Eur. Phys. J.* C24:459 (2002)
- [138] Klein SR, Nystrand J. *Phys. Rev. Lett.* 92:142003 (2004)
- [139] Deshpande A, Milner R, Venugopalan R, Vogelsang W. arXiv:hep-ph/0506148